Reexamining $B \to \pi\pi, \pi K$ decays in QCD factorization approach

Xinqiang Li[1,2,3] and Yadong Yang[1,*]

[1]*Department of Physics, Henan Normal University, Xinxiang, Henan 453007, People's Republic of China*
[2]*Institute of Theoretical Physics, Chinese Academy of Sciences, Beijing, 100080, People's Republic of China*
[3]*Graduate School of the Chinese Academy of Science, Beijing, 100039, People's Republic of China*

Motivated by the recent experimental data, we have revisited the $B \to \pi K$, $\pi\pi$ decays in the framework of QCD factorization, with inclusion of the important strong penguin corrections of order α_s^2 induced by $b \to Dg^*g^*$ ($D = d$ or s and g^* denotes an off-shell gluon) transitions. We find that these higher order strong penguin contributions can provide $\sim 30\%$ enhancement to the penguin-dominated $B \to \pi K$ decay rates, and such an enhancement can improve the consistency between the theoretical predictions and the experimental data significantly, while for the tree-dominated $B \to \pi\pi$ decays, these higher order contributions play only a minor role. When these strong penguin contributions are summed, only a small strong phase remains and the direct CP asymmetries get small corrections. We also find that patterns of the ratios between the CP-averaged branching fractions remain nearly unaffected even after including these higher order corrections and the πK puzzle still persists. Our results may indicate that to resolve the puzzle one would have to resort to new physics contributions in the electroweak penguin sector as found by Buras *et al.*

I. INTRODUCTION

The study of exclusive hadronic B-meson decays can provide not only an interesting avenue to understand the CP violation and flavor mixing of the quark sector in the standard model (SM), but also powerful means to probe different new physics scenarios beyond the SM. With the operation of B-factory experiments, large amounts of experimental data on hadronic B-meson decays are being collected and measurements of previously known observables are becoming more and more precise. Thus, studies of the hadronic B-meson decays have entered a precision era.

With respect to the theoretical aspect, several novel methods have also been proposed to study exclusive hadronic B decays, such as the "naive" factorization (NF) [1], the perturbative QCD method (pQCD) [2], the QCD factorization (QCDF) [3,4], the soft collinear effective theory (SCET) [5], and so on. For quite a long time, the decay amplitudes for exclusive two-body hadronic B decays were estimated in the NF approach, and in many cases, this approach could provide the correct order of the magnitude of the branching fractions. However, it cannot predict the direct CP asymmetries properly due to the assumption of no strong rescattering in the final states. It is therefore no longer adequate to account for the new B-factory data. The other methods mentioned above are proposed to supersede this conventional approach. Since we shall use QCDF approach in this paper, we would only focus on this approach below.

The essence of the QCDF approach can be summarized as follows: since the b quark mass is much larger than the strong-interaction scale Λ_{QCD}, in the heavy-quark limit $m_b \gg \Lambda_{\mathrm{QCD}}$, the hadronic matrix elements relevant to two-body hadronic B-meson decays can be represented in the factorization form [3]

$$\langle M_1(p_1)M_2(p_2)|Q_i|B(p)\rangle = \langle M_1(p_1)|j_1|B(p)\rangle\langle M_2(p_2)|j_2|0\rangle\left[1 + \sum r_n \alpha_s^n + \mathcal{O}(\Lambda_{\mathrm{QCD}}/m_b)\right], \tag{1}$$

where Q_i is the local four-quark operator in the effective weak Hamiltonian, $j_{1,2}$ are bilinear quark currents, and M_1 is the meson that picks up the spectator quark from the B meson, while M_2 is the one that can be factored out from the (B, M_1) system. This scheme has incorporated elements of the NF approach (as the leading contribution) and the hard-scattering approach (as the subleading corrections).

It provides a means to compute the hadronic matrix elements systematically. In particular, the final-state strong-interaction phases, which are very important for studying CP violation in B-meson decays, are calculable from first principles with this formalism. Its accuracy is limited only by higher order power corrections to the heavy-quark limit and the uncertainties of theoretical input parameters such as quark masses, form factors, and the light-cone distribution amplitudes. Details about the conceptual foundations and the arguments of this approach could be found in Refs. [3,4].

*Corresponding author.
Email address: yangyd@henannu.edu.cn.

Among the two-body hadronic B-meson decays, the charmless $B \to \pi K$ and $B \to \pi\pi$ modes are very interesting, since a significant interference of tree and penguin amplitudes is expected, and hence have been studied most extensively. Experimentally, all four decay channels for $B \to \pi K$ ($B^{\pm} \to \pi^{\pm} K^0$, $B^{\pm} \to \pi^0 K^{\pm}$, $B^0 \to \pi^{\pm} K^{\mp}$, and $B^0 \to K^0 \pi^0$) and the three for $B \to \pi\pi$ ($B^{\pm} \to \pi^{\pm}\pi^0$, $B^0 \to \pi^+\pi^-$, and $B^0 \to \pi^0\pi^0$) have been observed with the CP-averaged branching ratios measured within a few percent errors by the CLEO [6–8], *BABAR* [9], and Belle [10] collaborations. The CP asymmetries in these decay modes have also been measured recently [11–19]. In particular, measurements of the direct CP asymmetry in $B^0 \to \pi^{\pm} K^{\mp}$ have been recently achieved at the 5.7σ level by *BABAR* [13,14] and Belle [15–17,20]. All these experimental data can therefore provide very useful information for improving the existing model calculations. On the theoretical side, these decay modes have also been analyzed in detail within the QCDF formalism [21–24]. Because of lack of precise experimental data at that time, no large discrepancies between the theoretical predictions and the experimental data were found. However, the current new B-factory data for $B \to \pi K$, $\pi\pi$ decays indicate some potential inconsistencies with the predictions based on this scheme. For example, new experimental data for $B^0 \to \pi^0 K^0$, $\pi^0\pi^0$ decay rates are significantly larger than the theoretical predictions with this scheme. In addition, predictions for the direct CP asymmetries in these modes are also inconsistent with the data, even with the opposite sign for some processes [21,25]. Moreover, the experimental results of the following ratios between the CP-averaged branching fractions for $B \to \pi K$, $\pi\pi$ decays [26,27]

$$R_{+-} \equiv 2\left[\frac{\text{BR}(B^+ \to \pi^+\pi^0) + \text{BR}(B^- \to \pi^-\pi^0)}{\text{BR}(B^0_d \to \pi^+\pi^-) + \text{BR}(\bar{B}^0_d \to \pi^+\pi^-)}\right]\frac{\tau_{B^0_d}}{\tau_{B^+}}$$
$$= 2.20 \pm 0.31, \tag{2}$$

$$R_{00} \equiv 2\left[\frac{\text{BR}(B^0_d \to \pi^0\pi^0) + \text{BR}(\bar{B}^0_d \to \pi^0\pi^0)}{\text{BR}(B^0_d \to \pi^+\pi^-) + \text{BR}(\bar{B}^0_d \to \pi^+\pi^-)}\right]$$
$$= 0.67 \pm 0.14, \tag{3}$$

$$R \equiv \left[\frac{\text{BR}(B^0_d \to \pi^- K^+) + \text{BR}(\bar{B}^0_d \to \pi^+ K^-)}{\text{BR}(B^+ \to \pi^+ K^0) + \text{BR}(B^- \to \pi^- \bar{K}^0)}\right]\frac{\tau_{B^+}}{\tau_{B^0_d}}$$
$$= 0.82 \pm 0.06, \tag{4}$$

$$R_{\text{c}} \equiv 2\left[\frac{\text{BR}(B^+ \to \pi^0 K^+) + \text{BR}(B^- \to \pi^0 K^-)}{\text{BR}(B^+ \to \pi^+ K^0) + \text{BR}(B^- \to \pi^- \bar{K}^0)}\right]$$
$$= 1.00 \pm 0.09, \tag{5}$$

$$R_{\text{n}} \equiv \frac{1}{2}\left[\frac{\text{BR}(B^0_d \to \pi^- K^+) + \text{BR}(\bar{B}^0_d \to \pi^+ K^-)}{\text{BR}(B^0_d \to \pi^0 K^0) + \text{BR}(\bar{B}^0_d \to \pi^0 \bar{K}^0)}\right]$$
$$= 0.79 \pm 0.08, \tag{6}$$

with numerical results compiled by the Heavy Flavor Averaging Group (HFAG) [28], have shown very puzzling patterns [29,30]. Within the SM, predictions based on the QCDF approach give $R_c \approx R_n$, while the value for R is quite consistent with the experimental data [25]. The central values for R_{+-} and R_{00} calculated with the QCD factorization [25] give $R_{+-} = 1.24$ and $R_{00} = 0.07$ as emphasized by Buras *et al.*[30], which are also inconsistent with the current experimental data. Though none of these exciting results is conclusive at the moment due to large uncertainties both theoretically and experimentally, it is important and interesting to take them seriously and to find out possible origins of these discrepancies. Recently, quite a lot of works have been done to study the implications of these new experimental data [30–41]. In this paper, we restrict ourselves to the possibility that these deviations result from our insufficient understanding of the hadronic dynamics and investigate the higher order strong penguin effects induced by $b \to Dg^*g^*$ transitions, where $D = d$ or s depends on the specific decay modes. The off-shell gluons g^* are either emitted from the internal quark loops, external quark lines, or split off from the virtual gluon of the strong penguin.

As shown in the literature [42–47], contributions of the higher order $b \to sgg$ process to the inclusive and semi-inclusive decay rates of B-meson decays could be large compared to the $b \to sg$ process. For example, in [45], Greub and Liniger have found that the next-to-leading logarithmic result of $\mathcal{B}^{\text{NLL}}(b \to sg) = (5.0 \pm 1.0) \times 10^{-5}$ is more than a factor of 2 larger than the leading logarithmic one $\mathcal{B}^{\text{LL}}(b \to sg) = (2.2 \pm 0.8) \times 10^{-5}$. In addition, in [47], we have found the higher order strong penguin could give large corrections to $B \to \phi X_s$. We also note that the large higher order chromo-magnetic penguin contributions have also been found by Mishima and Sanda [48] in the pQCD factorization framework. Since the $B \to \pi K$ decays are dominated by strong penguin contributions, it is interesting to investigate these higher order $b \to sg^*g^*$ strong penguin effects on these penguin-dominated processes. However, for consistency, we will also investigate these effects on the tree-dominated $B \to \pi\pi$ decays. After direct calculations, we find that these higher order strong penguin contributions can provide $\sim 30\%$ enhancement to the penguin-dominated $B \to \pi K$ decay rates, and such an enhancement can improve the consistency between the theoretical predictions and the experimental data effectively. For tree-dominated $B \to \pi\pi$ decays, however, their effects are quite small. Since the $b \to Dg^*g^*$ strong penguin contributions contain only a relatively small strong phase, their effects on the direct CP asymmetries are also small. In addition, the patterns of the quantities R, R_c, R_n,

R_{+-}, and R_{00} defined above remain unaffected even with these new contributions included.

This paper is organized as follows: In Sec. II, using the QCDF approach, we first calculate the $B \to \pi K$, $\pi\pi$ decay amplitudes at the next-to-leading order in α_s, and then take into account the $b \to D g^* g^*$ strong penguin contributions to the decay amplitudes. In Sec. III, after presenting the theoretical input parameters relevant to our analysis, we give our numerical results for $B \to \pi K$ and $B \to \pi\pi$ decays. Some discussions on these higher order corrections and the γ dependence of the relevant quantities are also presented. Finally, we conclude with a summary in Sec. IV. In Appendix A, we present the correction functions at next-to-leading order in α_s. Explicit forms for the quark loop functions are given in Appendix B.

II. DECAY AMPLITUDES FOR $B \to \pi K$, $\pi\pi$ DECAYS IN QCDF APPROACH

A. The effective weak Hamiltonian for hadronic B decays

In phenomenological treatment of the hadronic B-meson decays, the starting point is the effective weak Hamiltonian at the low energy [49,50], which is obtained by integrating out the heavy degree of freedom (e.g. the top quark, $W^{\pm}$ and Z bosons in the SM) from the Lagrangian of the full theory. After using the unitarity relation $-\lambda_t = \lambda_u + \lambda_c$, it can be written as

$$
\mathcal{H}_{\text{eff}} = \frac{G_F}{\sqrt{2}} \sum_{p=u,c} \lambda_p^{(\prime)} \left(C_1 Q_1^p + C_2 Q_2^p + \sum_{i=3,...,10} C_i Q_i \right.
$$
$$
\left. + C_{7\gamma} Q_{7\gamma} + C_{8g} Q_{8g} \right) + \text{H.c.}, \quad (7)
$$

where $\lambda_p = V_{pb} V_{ps}^*$ (for $b \to s$ transition) and $\lambda_p' = V_{pb} V_{pd}^*$ (for $b \to d$ transition) are products of the Cabibbo-Kobayashi-Maskawa (CKM) matrix elements. The effective operators Q_i govern a given decay process and their explicit form can be read as follows.

(i) Current-current operators:

$$
\begin{aligned}
Q_1^p &= (\bar{p}b)_{V-A}(\bar{D}p)_{V-A}, \\
Q_2^p &= (\bar{p}_i b_j)_{V-A}(\bar{D}_j p_i)_{V-A},
\end{aligned} \quad (8)
$$

(ii) QCD-penguin operators:

$$
\begin{aligned}
Q_3 &= (\bar{D}b)_{V-A}\sum_q (\bar{q}q)_{V-A}, \\
Q_4 &= (\bar{D}_i b_j)_{V-A}\sum_q (\bar{q}_j q_i)_{V-A}, \\
Q_5 &= (\bar{D}b)_{V-A}\sum_q (\bar{q}q)_{V+A}, \\
Q_6 &= (\bar{D}_i b_j)_{V-A}\sum_q (\bar{q}_j q_i)_{V+A},
\end{aligned} \quad (9)
$$

(iii) Electroweak penguin operators:

$$
\begin{aligned}
Q_7 &= (\bar{D}b)_{V-A}\sum_q \frac{3}{2} e_q (\bar{q}q)_{V+A}, \\
Q_8 &= (\bar{D}_i b_j)_{V-A}\sum_q \frac{3}{2} e_q (\bar{q}_j q_i)_{V+A}, \\
Q_9 &= (\bar{D}b)_{V-A}\sum_q \frac{3}{2} e_q (\bar{q}q)_{V-A}, \\
Q_{10} &= (\bar{D}_i b_j)_{V-A}\sum_q \frac{3}{2} e_q (\bar{q}_j q_i)_{V-A},
\end{aligned} \quad (10)
$$

(iv) Electro- and chromo-magnetic dipole operators:

$$
\begin{aligned}
Q_{7\gamma} &= \frac{-e}{8\pi^2} m_b \bar{D}\sigma_{\mu\nu}(1+\gamma_5)F^{\mu\nu}b, \\
Q_{8g} &= \frac{-g_s}{8\pi^2} m_b \bar{D}\sigma_{\mu\nu}(1+\gamma_5)G^{\mu\nu}b,
\end{aligned} \quad (11)
$$

where $(\bar{q}_1 q_2)_{V\pm A} = \bar{q}_1 \gamma_\mu (1 \pm \gamma_5) q_2$, i, j are color indices, e_q are the electric charges of the quarks in units of $|e|$, and a summation over $q = u, d, s, c, b$ is implied. For decay modes induced by the quark level $b \to d$ transition, $D = d$, while for $b \to s$ transition, $D = s$.

The Wilson coefficients $C_i(\mu)$ in Eq. (7) represent all the contributions from physics with scale higher than $\mu \sim \mathcal{O}(m_b)$ and have been reliably evaluated up to the next-to-leading logarithmic order. Numerical results for these coefficients evaluated at different scales can be found in [49].

B. Decay amplitudes at the next-to-leading order in α_s

Using the weak effective Hamiltonian given by Eq. (7), we can now write the decay amplitudes for the general two-body hadronic $B \to M_1 M_2$ decays as

$$
\langle M_1 M_2 | \mathcal{H}_{\text{eff}} | B \rangle = \frac{G_F}{\sqrt{2}} \sum_{p=u,c} \lambda_p C_i \langle M_1 M_2 | Q_i^p | B \rangle. \quad (12)
$$

Then, the most essential theoretical problem obstructing the calculation of the hadronic B-meson decay amplitudes resides in the evaluation of the hadronic matrix elements of the local operators $\langle M_1 M_2 | Q_i^p | B \rangle$. Within the formalism of the QCDF, this quantity could be simplified greatly in the heavy-quark limit. To leading power in Λ_{QCD}/m_b, but to all orders in perturbation theory, it obeys the following factorization formula [21],

$$
\begin{aligned}
\langle M_1 M_2 | Q_i^p | B \rangle = &\, F_j^{B \to M_1}(m_{M_2}^2) \times T_{M_2,ij}^{\text{I}} * \Phi_{M_2} \\
&+ F_j^{B \to M_2}(m_{M_1}^2) \times T_{M_1,ij}^{\text{I}} * \Phi_{M_1} \\
&+ T_i^{\text{II}} * \Phi_B * \Phi_{M_1} * \Phi_{M_2}, \quad (13)
\end{aligned}
$$

where Φ_M is the leading-twist light-cone distribution amplitude of the meson M, and the $*$ products indicate an

integration over the light-cone momentum fractions of the constituent quarks inside the mesons. The quantity $F_j^{B \to M}$ denotes the $B \to M$ transition form factor. This formula is illustrated by the graphs shown in Fig. 1.

In Eq. (13), the hard-scattering kernels $T_{M,ij}^{\mathrm{I}}$ and T_i^{II} are calculable order by order with the perturbation theory. $T_{M,ij}^{\mathrm{I}}$ starts at tree level, and at higher order in α_s contains the "nonfactorizable" corrections from the hard gluon exchange and the light-quark loops (penguin topologies). The hard "nonfactorizable" interactions involving the spectator quark are part of the kernel T_i^{II}. At the leading order, $T_{M,ij}^{\mathrm{I}} = 1$, $T_i^{\mathrm{II}} = 0$, and the QCDF formula reproduce the NF results. Nonperturbative effects are either suppressed by $\Lambda_{\mathrm{QCD}}/m_b$ or parametrized in terms of the meson decay constants, the transition form factors $F_j^{B \to M}$, and the light-cone distribution amplitudes Φ_B, Φ_M. The relevant Feynman diagrams contributing to these kernels at the next-to-leading in α_s are shown in Fig. 2.

According to the arguments in [3], the weak annihilation contributions to the decay amplitudes are power suppressed compared to the leading spectator interaction in the heavy-quark limit, and hence do not appear in the factorization formula (13). Nevertheless, as emphasized in [2,51,52], these contributions may be numerically important for realistic B-meson decays. In particular, the annihilation contributions with QCD corrections could give potentially large strong phases, hence large CP violation could be expected [2,51]. It is therefore necessary to

take these annihilation contributions into account. At leading order in α_s, the annihilation kernels arise from the four diagrams shown in Fig. 3. They result in a further contribution to the hard-scattering kernel T_i^{II} in the factorization formula.

As indicated in the factorization formula (13), the meson light-cone distribution amplitudes (LCDAs) play an important role in the QCDF formalism. For convenience, we list the relevant formula as follows (details can be found in [53]).

LCDAs for B meson.—In the heavy-quark limit, the light-cone projector for the B meson in the momentum space can be expressed as [3,53,54]

$$\mathcal{M}_{\alpha\beta}^B = -\frac{if_B m_B}{4} \big[(1 + \not{p})\gamma_5 \{\Phi_1^B(\xi) + \not{n}_- \Phi_2^B(\xi)\}\big]_{\beta\alpha},$$

(14)

with the normalization condition

$$\int_0^1 d\xi \Phi_1^B(\xi) = 1, \qquad \int_0^1 d\xi \Phi_2^B(\xi) = 0, \quad (15)$$

where ξ is the momentum fraction of the spectator quark in the B meson. For simplicity, we consider only the leading-twist $\Phi_1^B(\xi)$ contribution in this paper. Since almost all the momentum of the B meson is carried by the heavy b quark, we expect that $\Phi_1^B(\xi) = \mathcal{O}(m_b/\Lambda_{\mathrm{QCD}})$ and $\xi = \mathcal{O}(\Lambda_{\mathrm{QCD}}/m_b)$.

LCDAs for light mesons.—For the light-cone projector of light pseudoscalar mesons in momentum space, we use the form given by [55]

$$M_{\alpha\beta}^P = \frac{if_P}{4}\left\{\not{p}\gamma_5 \Phi(x) - \mu_P \gamma_5 \frac{\not{k}_2 \not{k}_1}{k_1 \cdot k_2} \Phi_p(x)\right\}_{\alpha\beta}, \quad (16)$$

where f_P and p are the decay constant and the momentum of the meson. The parameter $\mu_P = m_P^2/(\overline{m}_1(\mu) + \overline{m}_2(\mu))$, with $\overline{m}_{1,2}(\mu)$ being the current quark mass of the meson constituents, is proportional to the chiral quark condensate. $\Phi(x)$ is the leading-twist distribution amplitude, whereas $\Phi_p(x)$ the sub-leading-twist (twist-3) one. All of them are normalized to 1. The quark and antiquark momenta of meson constituents, k_1 and k_2, are defined, respectively, by

$$k_1^\mu = xp^\mu + k_\perp^\mu + \frac{\vec{k}_\perp^2}{2xp \cdot \bar{p}} \bar{p}^\mu,$$

$$k_2^\mu = (1 - x)p^\mu - k_\perp^\mu + \frac{\vec{k}_\perp^2}{2(1 - x)p \cdot \bar{p}} \bar{p}^\mu,$$

(17)

where $\bar{p}$ is a lightlike vector whose 3-components point

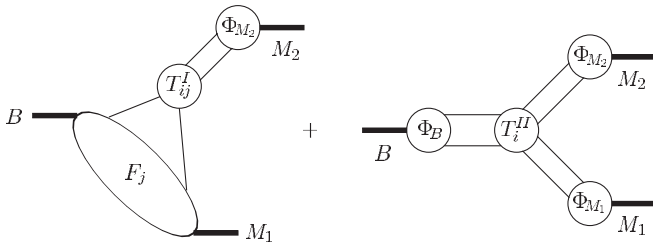FIG. 1. Graphical representation of the factorization formula. Only one of the two form-factor terms in (13) is shown for simplicity.

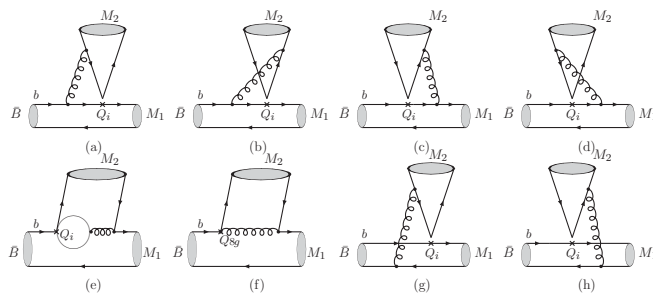FIG. 2. Order α_s corrections to the hard-scattering kernels $T_{M,ij}^{\mathrm{I}}$ [coming from the diagrams (a)–(f)] and T_i^{II} (from the last two diagrams).
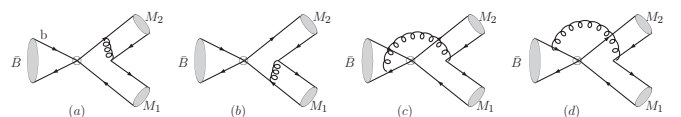

FIG. 3. The annihilation diagrams of order α_s.

into the opposite direction of $\vec{p}$. It is understood that only after the factor $k_1 \cdot k_2$ in the denominator of Eq. (16) canceled can we take the collinear approximation, i.e., the momentum k_1 and k_2 can be set to xp and $(1-x)p$, respectively.

From now on, we denote by u the longitudinal momentum fraction of the constituent quark in the emitted meson M_2, which can be factored out from the (B, M_1) system, and by v the momentum fraction of the quark in the

recoiled meson M_1, which picks up the spectator quark from the decaying B meson. For the B meson decaying into two light energetic hadronic final states, we define the light-cone distribution amplitudes by choosing the $+$ direction along the decay path of the emission meson M_2.

Equipped with these necessary preliminaries, the four $B \to \pi K$ and the three $B \to \pi\pi$ decay amplitudes can be expressed as [21,25]

$$
\mathcal{A}(B^- \to \pi^- \overline{K}^0) = \lambda_p\left[\left(a_4^p - \frac{1}{2}a_{10}^p\right) + r_\chi^K\left(a_6^p - \frac{1}{2}a_8^p\right)\right]X^{(B^-\pi^-,\overline{K}^0)} + [\lambda_u b_2 + (\lambda_u + \lambda_c)(b_3 + b_3^{\mathrm{ew}})]X^{(B^-,\pi^-\overline{K}^0)},
$$

$$
\sqrt{2}\mathcal{A}(B^- \to \pi^0 K^-) = [\lambda_u a_1 + \lambda_p(a_4^p + a_{10}^p) + \lambda_p r_\chi^K(a_6^p + a_8^p)]X^{(B^-\pi^0,K^-)} + \left[\lambda_u a_2 + \lambda_p \frac{3}{2}(-a_7^p + a_9^p)\right]X^{(B^-K^-,\pi^0)}
$$

$$
+ [\lambda_u b_2 + (\lambda_u + \lambda_c)(b_3 + b_3^{\mathrm{ew}})]X^{(B^-,\pi^0 K^-)},
$$

$$
\mathcal{A}(\overline{B}^0 \to \pi^+ K^-) = [\lambda_u a_1 + \lambda_p(a_4^p + a_{10}^p) + \lambda_p r_\chi^K(a_6^p + a_8^p)]X^{(\overline{B}^0\pi^+,K^-)} + (\lambda_u + \lambda_c)\left(b_3 - \frac{1}{2}b_3^{\mathrm{ew}}\right)X^{(\overline{B}^0,\pi^+ K^-)},
$$

$$
\sqrt{2}\mathcal{A}(\overline{B}^0 \to \pi^0\overline{K}^0) = \left[\lambda_u a_2 + \lambda_p \frac{3}{2}(-a_7^p + a_9^p)\right]X^{(\overline{B}^0\overline{K}^0,\pi^0)} - \lambda_p\left[\left(a_4^p - \frac{1}{2}a_{10}^p\right) + r_\chi^K\left(a_6^p - \frac{1}{2}a_8^p\right)\right]X^{(\overline{B}^0\pi^0,\overline{K}^0)}
$$

$$
- (\lambda_u + \lambda_c)\left(b_3 - \frac{1}{2}b_3^{\mathrm{ew}}\right)X^{(\overline{B}^0,\pi^0\overline{K}^0)}, \tag{18}
$$

$$
\mathcal{A}(\overline{B}^0 \to \pi^+ \pi^-) = [\lambda_u' a_1 + \lambda_p'(a_4^p + a_{10}^p) + \lambda_p' r_\chi^\pi(a_6^p + a_8^p)]X^{(\overline{B}^0\pi^+,\pi^-)}
$$

$$
+ \left[\lambda_u' b_1 + (\lambda_u' + \lambda_c')\left(b_3 + 2b_4 - \frac{1}{2}b_3^{\mathrm{ew}} + \frac{1}{2}b_4^{\mathrm{ew}}\right)\right]X^{(\overline{B}^0,\pi^+\pi^-)},
$$

$$
\sqrt{2}\mathcal{A}(B^- \to \pi^- \pi^0) = \left[\lambda_u'(a_1 + a_2) + \frac{3}{2}\lambda_p'(-a_7^p + r_\chi^\pi a_8^p + a_9^p + a_{10}^p)\right]X^{(B^-\pi^-,\pi^0)},
$$

$$
\mathcal{A}(\bar{B}^0 \to \pi^0\pi^0) = \left[-\lambda_u' a_2 + \lambda_p'\left(a_4^p - \frac{1}{2}a_{10}^p\right) + \lambda_p' r_\chi^\pi\left(a_6^p - \frac{1}{2}a_8^p\right) - \frac{3}{2}\lambda_p'(-a_7^p + a_9^p)\right]X^{(\overline{B}^0\pi^0,\pi^0)}
$$

$$
+ \left[\lambda_u' b_1 + (\lambda_u' + \lambda_c')\left(b_3 + 2b_4 - \frac{1}{2}b_3^{\mathrm{ew}} + \frac{1}{2}b_4^{\mathrm{ew}}\right)\right]X^{(\overline{B}^0,\pi^0\pi^0)}, \tag{19}
$$

where the "chirally enhanced" factor $r_\chi^M = r_\chi^M(\mu)$ associated with the coefficients a_6 and a_8 is defined by

$$
r_\chi^K(\mu) = \frac{2m_K^2}{\overline{m}_b(\mu)(\overline{m}_{u,d}(\mu) + \overline{m}_s(\mu))},
$$

$$
r_\chi^\pi(\mu) = \frac{2m_\pi^2}{\overline{m}_b(\mu)(\overline{m}_u(\mu) + \overline{m}_d(\mu))}, \tag{20}
$$

with $\overline{m}_q(\mu)$ being the current quark mass and depending on the scale μ. The CP-conjugated decay amplitudes are obtained from the above expressions by just replacing $\lambda_p^{(l)}$ with $\lambda_p^{(l)*}$.

In Eqs. (18) and (19), we have defined $X^{(\bar{B}M_1, M_2)}$ as the factorized amplitude with the meson M_2 being factored out from the $(\bar{B}, M_1)$ system

$$
X^{(\bar{B}M_1, M_2)} = \langle M_2|(\bar{q}_2 q_3)_{V-A}|0\rangle \cdot \langle M_1|(\bar{q}_1 b)_{V-A}|\bar{B}\rangle. \tag{21}
$$

In term of the decay constant and the transition form factors defined by [53,56]

$$
\langle M(p)|\bar{q}\gamma_\mu\gamma_5 q'|0\rangle = -if_P p_\mu, \tag{22}
$$

$$
\langle M(p')|\bar{q}\gamma^\mu b|\bar{B}(p)\rangle = F_+^{\bar{B}\to M}(q^2)\left[p^\mu + p'^\mu\right.
$$

$$
\left. - \frac{m_B^2 - m_M^2}{q^2}q^\mu\right]
$$

$$
+ F_0^{\bar{B}\to M}(q^2)\frac{m_B^2 - m_M^2}{q^2}q^\mu, \tag{23}
$$

the factorized amplitude can be written as

$$
X^{(\bar{B}M_1, M_2)} = i\frac{G_F}{\sqrt{2}}(m_B^2 - m_{M_1}^2)F_0^{\bar{B}\to M_1}(m_{M_2}^2)f_{M_2}, \tag{24}
$$

where we have combined the factor $\frac{G_F}{\sqrt{2}}$ in the effective Hamiltonian. The quantity $X^{(\bar{B}, M_1 M_2)}$ associated with the

annihilation coefficient b_i and b_i^{ew} is given by

$$X^{(\bar{B},M_1M_2)} = i\frac{G_F}{\sqrt{2}}f_B f_{M_1} f_{M_2}. \qquad (25)$$

The parameters $a_i \equiv a_i(M_1M_2)$ in Eqs. (18) and (19) encode all the "nonfactorizable" corrections up to next-to-leading order in α_s, and are calculable with perturbative theory. The general form of these coefficients a_i^p can be written as [25]

$$a_i^p(M_1M_2) = \left(C_i + \frac{C_{i\pm1}}{N_c}\right) + \frac{C_{i\pm1}}{N_c}\frac{C_F\alpha_s}{4\pi}\left[V_i(M_2)\right.$$
$$\left. + \frac{4\pi^2}{N_c}H_i(M_1M_2)\right] + P_i^p(M_2), \qquad (26)$$

where $C_F = (N_C^2 - 1)/(2N_C)$, and $N_C = 3$ is the number of colors. The upper (lower) signs apply when i is odd (even) and the superscript "p" should be omitted for $i = 1, 2$. The first part in Eq. (26) corresponds to the NF results, and the remaining ones to the corrections up to the next-to-leading order in α_s. The quantities $V_i(M_2)$ account for the one-loop vertex corrections, $H_i(M_1M_2)$ for the hard spectator interactions, and $P_i^p(M_1M_2)$ for the penguin contractions. In general, these quantities can be written as the convolution of the hard-scattering kernels with the meson distribution amplitudes. Explicit forms for these quantities are relegated to Appendix A.

The parameters $b_i \equiv b_i(M_1M_2)$ in Eqs. (18) and (19) correspond to the weak annihilation contributions and are given as [25]

$$b_1 = \frac{C_F}{N_c^2}C_1 A_1^i,$$
$$b_3 = \frac{C_F}{N_c^2}[C_3 A_1^i + C_5(A_3^i + A_3^f) + N_c C_6 A_3^f], \qquad (27)$$

$$b_2 = \frac{C_F}{N_c^2}C_2 A_1^i, \qquad b_4 = \frac{C_F}{N_c^2}[C_4 A_1^i + C_6 A_2^i], \qquad (28)$$

$$b_3^{\text{ew}} = \frac{C_F}{N_c^2}[C_9 A_1^i + C_7(A_3^i + A_3^f) + N_c C_8 A_3^f], \qquad (29)$$

$$b_4^{\text{ew}} = \frac{C_F}{N_c^2}[C_{10} A_1^i + C_8 A_2^i], \qquad (30)$$

where we have omitted the argument "M_1M_2." These coefficients correspond to the current-current annihilation (b_1, b_2), the penguin annihilation (b_3, b_4), and the electroweak penguin annihilation (b_3^{ew}, b_4^{ew}), respectively. The explicit form for the building blocks $A_k^{i,j}$ can be found in Appendix A.

It should be noted that within the QCDF framework, all the nonfactorizable power suppressed contributions except for the hard spectator and the annihilation contributions are neglected. We have rederived the above next-to-leading

order formulas calculated by Beneke and Neubert [25], for which no deviation has been found.

C. The $b \to Dg^*g^*$ strong penguin contributions to the $B \to \pi K$, $\pi\pi$ decays

From the previous subsection, we can see that, up to next-to-leading order in α_s and to leading power in Λ_{QCD}/m_b, the strong-interaction phases originate from the imaginary parts of the functions $g(u)$ and $G(s, u)$, as defined in Eq. (A2) and Eq. (A8), respectively. The presence of a strong-interaction phase in the penguin function $G(s, u)$ is well known and commonly referred to as the Bander-Silverman-Soni (BSS) mechanism [57]. The reliable calculation of the imaginary part of function $g(u)$ arising from the hard gluon exchanging between the two outgoing mesons is a new product of the QCDF approach. However, recent experimental data indicate that there may exist extra new strong-interaction phases in hadronic B-meson decays. Since the $b \to sgg$ transitions play an important role in the inclusive and semi-inclusive B-meson decays as discussed in the literature [42–48], in this section we shall generalize these results to exclusive two-body hadronic B decays, and investigate these $b \to Dg^*g^*$ strong penguin contributions to $B \to \pi K$, $\pi\pi$ decays.

At the quark level, the $b \to Dg^*g^*$ transitions can occur in many different manners as depicted by Figs. 4–6. For example, one of the gluons can radiate from the external quark line, with the other one coming from the chromo-magnetic dipole operator O_{8g} as in Figs. 5(b) and 5(c) or from the internal quark loop in the QCD-penguin diagrams in Figs. 6(b) and 6(c). On the other hand, the two gluons can also radiate from the internal quark loops in Figs. 6(d) and 6(e) or split off the virtual gluon of the strong penguin processes as shown by Figs. 5(a) and 6(a). Here we do not consider the diagrams of the category in Fig. 4, since their contributions can be absorbed into the definition of the $B \to M_1$ transition form factors Figs. 4(a) and 4(b) or further suppressed by $g_s^2/16\pi^2$. It is easy to clarify this
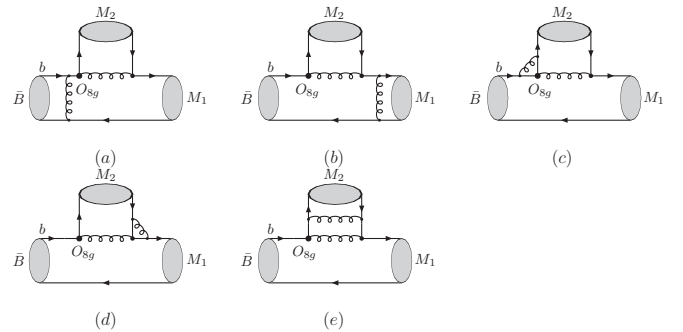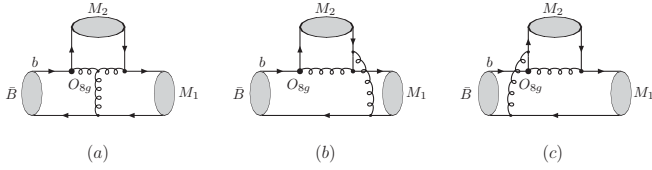

FIG. 4. Representative diagrams induced by the $b \to Dg^*g^*$ transition which are not evaluated. Here we give only the chromo-magnetic dipole operator Q_{8g} contributions. With $\mathcal{O}_{8g}$ replaced by the other operators, the corresponding diagrams for these operators can also be obtained.

FIG. 5. Chromo-magnetic operator Q_{8g} contributions induced by the $b \to Dg^*g^*$ transition.

FIG. 6. Strong penguin contributions induced by the $b \to Dg^*g^*$ transition.

point by comparing the strengths of Fig. 4(c) to that of Fig. 5(a).

As can be seen from Figs. 5 and 6, these penguin diagrams should be the dominant contributions of order α_s^2, *since they are not two-loop QCD diagrams and there is no additional $\frac{1}{16\pi^2}$ suppression factor compared to the genuine two-loop contributions of order α_s^2.* Studies of these contributions could be helpful for understanding the higher order perturbative corrections within the QCDF formalism. In the following, we first discuss these higher order strong penguin contributions to decay modes with two light pseudoscalar mesons in the final states,
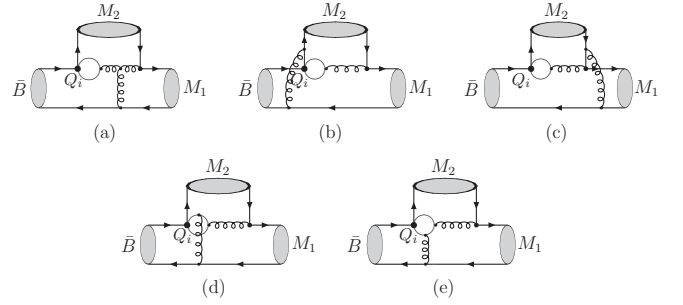
$B \to M_1 M_2$, and then specialize this general case to the $B \to \pi K, \pi\pi$ decays and investigate the effect of these higher order corrections on the branching ratios and *CP* asymmetries for these modes.

We start with the calculation of the diagrams in Fig. 5. In this case, the weak decay is induced by the chromo-magnetic dipole operator O_{8g}. The calculation is straightforward with the result given by

$$\mathcal{A}_{Q_{8g}} = -i\frac{\alpha_s^2 f_B f_{M_1} f_{M_2}}{N_c^3}\lambda_t^{(\prime)}\int_0^1 d\xi\,\frac{\Phi_1^B(\xi)}{\xi}\int_0^1 dudv\Bigg\{\Phi_{M_2}(u)\Phi_{M_1}(v)\Bigg[\frac{1}{6(1-u)(1-v)} + \frac{3(3-v)}{2(1-u)(1-v)v}\Bigg]$$
$$+ r_\chi^{M_1}\Phi_{M_2}(u)\Phi_p^{M_1}(v)\Bigg[\frac{2-u}{6(1-u)u(1-v)} + \frac{3(3-u-v+uv)}{2(1-u)^2(1-v)v}\Bigg]$$
$$+ r_\chi^{M_2}\Phi_p^{M_2}(u)\Phi_{M_1}(v)\Bigg[\frac{1+u}{6(1-u)(1-v)} + \frac{3(3-u-v-uv)}{2(1-u)(1-v)v}\Bigg]$$
$$+ r_\chi^{M_1}r_\chi^{M_2}\Phi_p^{M_2}(u)\Phi_p^{M_1}(v)\Bigg[\frac{1}{6(1-u)(1-v)} + \frac{3(3-v)}{2(1-u)(1-v)v}\Bigg]\Bigg\}, \tag{31}$$

where $\lambda_t = V_{tb}V_{ts}^*$ (for the $b \to s$ transition) and $\lambda_t' = V_{tb}V_{td}^*$ (for the $b \to d$ transition) are products of the CKM matrix elements. As always, Φ_M and Φ_p^M denote the leading-twist and twist-3 LCDAs of the pseudoscalar meson M in the final state, respectively.

In calculation of the Feynman diagrams of Fig. 6, we follow the method proposed by Greub and Liniger [45]. First, we calculate the fermion loops in these individual diagrams, and then insert these building blocks into the entire diagrams to obtain the total contributions. In evaluating the internal quark loop diagrams, we shall adopt the naive dimensional regularization (NDR) scheme and the modified minimal subtraction ($\overline{\text{MS}}$) scheme. In addition, we shall adopt the *ad hoc* Feynman gauge throughout this paper. Similar to the calculation of the penguin contractions in Appendix A, we should consider the two distinct contractions in the weak interaction vertex of these penguin diagrams.

As can be seen from Fig. 6, the first three diagrams have the same building block $I_\mu^a(k)$ (corresponding to the contraction of operators $Q_{1,3}$) or $\tilde{I}_\mu^a(k)$ (associated with the

contractions of the operators $Q_{4,6}$). These building blocks are shown in Fig. 7 and given by

$$I_\mu^a(k) = \frac{g_s}{4\pi^2}\Gamma\left(\frac{\epsilon}{2}\right)(2-\epsilon)(4\pi\mu^2)^{\epsilon/2}(k_\mu\slashed{k} - k^2\gamma_\mu)$$
$$\times (1-\gamma_5)T^a\int_0^1 dx\,\frac{x(1-x)}{[m_q^2 - x(1-x)k^2 - i\delta]^{\epsilon/2}}, \tag{32}$$
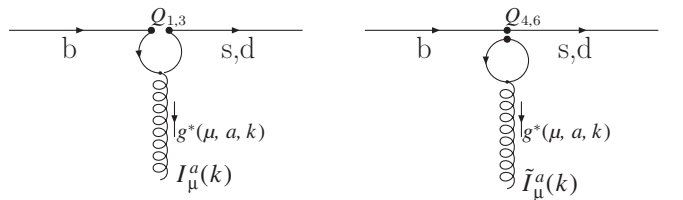
FIG. 7. Building blocks $I_\mu^a(k)$ (associated with the contraction of the operators $Q_{1,3}$) and $\tilde{I}_\mu^a(k)$ (associated with the contraction of the operators $Q_{4,6}$) for Figs. 6(a)–6(c).

$$\tilde{I}_\mu^a(k) = \frac{g_s}{2\pi^2}\Gamma\left(\frac{\epsilon}{2}\right)(4\pi\mu^2)^{\epsilon/2}(k_\mu\slashed{k} - k^2\gamma_\mu)(1 - \gamma_5)$$

$$\times T^a \int_0^1 dx \frac{x(1-x)}{[m_q^2 - x(1-x)k^2 - i\delta]^{\epsilon/2}}, \qquad (33)$$

where k and T^a are the momentum and the color generator of the off-shell gluon, g_s is the strong coupling constant, and m_q the pole mass of the quark propagating in the quark loops. The free indices μ and a should be contracted with the gluon propagator when inserting these building blocks into the entire diagrams. Here we have used the d dimension space-time as $d = 4 - \epsilon$. After performing the subtraction with the $\overline{\text{MS}}$ scheme, we get

$$I_\mu^a(k) = \frac{g_s}{8\pi^2}\left[-\frac{2}{3} - \frac{4}{3}\ln\frac{m_b}{\mu} + G(s_q, 1 - u)\right]$$

$$\times (k_\mu\slashed{k} - k^2\gamma_\mu)(1 - \gamma_5)T^a, \qquad (34)$$

$$\tilde{I}_\mu^a(k) = \frac{g_s}{8\pi^2}\left[-\frac{4}{3}\ln\frac{m_b}{\mu} + G(s_q, 1 - u)\right]$$

$$\times (k_\mu\slashed{k} - k^2\gamma_\mu)(1 - \gamma_5)T^a, \qquad (35)$$

with the function $G(s, u)$ defined by Eq. (A8).

The sum of the fermion loops in the last two diagrams in Fig. 6 are denoted by the building block $J_{\mu\nu}^{ab}(k, p)$ (corresponding to the contraction of operators $Q_{1,3}$) or $\tilde{J}_{\mu\nu}^{ab}(k, p)$ (corresponding to the contraction of operators $Q_{4,6}$), as depicted by Fig. 8. Using the decomposition advocated by [44,45], these building blocks can be expressed as

$$J_{\mu\nu}^{ab}(k, p) = T_{\mu\nu}^+(k, p)\{T^a, T^b\} + T_{\mu\nu}^-(k, p)[T^a, T^b], \quad (36)$$

$$\tilde{J}_{\mu\nu}^{ab}(k, p) = \tilde{T}_{\mu\nu}^+(k, p)\{T^a, T^b\} + \tilde{T}_{\mu\nu}^-(k, p)[T^a, T^b], \qquad (37)$$

where the first part is symmetric, while the second one is antisymmetric with respect to the color structures of the two gluons. Here $k(p)$, $a(b)$, and $\mu(\nu)$ are the momentum, color, and polarization of the off-shell gluons. Below, we refer to the gluon with indices (ν, b, p) as the one connecting with the spectator quark from the B meson.

In the NDR scheme, after integrating over the (shifted) loop momentum, we can present the quantities $T_{\mu\nu}^\pm(k, p)$ and $\tilde{T}_{\mu\nu}^\pm(k, p)$ as [44,45]

$$T_{\mu\nu}^+(k, p) = \frac{\alpha_s}{4\pi}\left[E(\mu, \nu, k)\Delta i_5 + E(\mu, \nu, p)\Delta i_6\right.$$

$$- E(\mu, k, p)\frac{k_\nu}{k \cdot p}\Delta i_{23} - E(\mu, k, p)$$

$$\times \frac{p_\nu}{k \cdot p}\Delta i_{24} - E(\nu, k, p)\frac{k_\mu}{k \cdot p}\Delta i_{25}$$

$$\left. - E(\nu, k, p)\frac{p_\mu}{k \cdot p}\Delta i_{26}\right](1 - \gamma_5), \qquad (38)$$

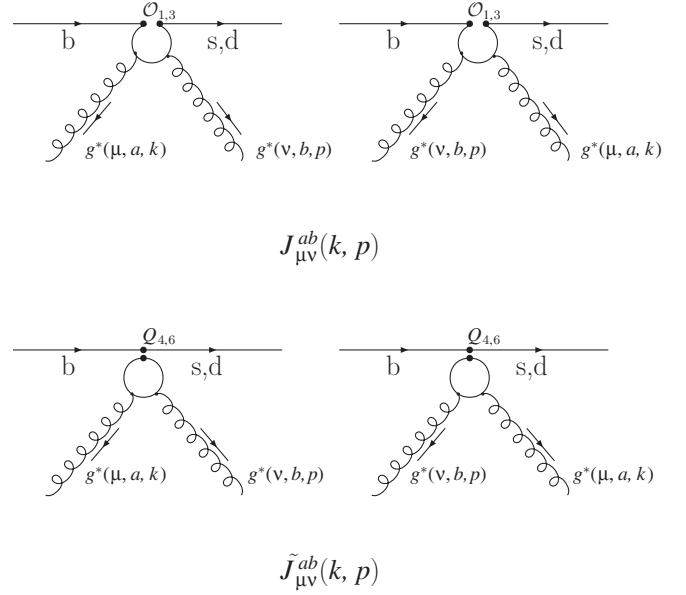$$J_{\mu\nu}^{ab}(k, p)$$

$$\tilde{J}_{\mu\nu}^{ab}(k, p)$$

FIG. 8. Building blocks $J_{\mu\nu}^{ab}(k, p)$ (associated with operators $Q_{1,3}$) and $\tilde{J}_{\mu\nu}^{ab}(k, p)$ (associated with operators $Q_{4,6}$) for Figs. 6(d) and 6(e).

$$T_{\mu\nu}^-(k, p) = \frac{\alpha_s}{4\pi}\left[\slashed{k}g_{\mu\nu}\Delta i_2 + \slashed{p}g_{\mu\nu}\Delta i_3 + \gamma_\mu k_\nu\Delta i_8\right.$$

$$+ \gamma_\mu p_\nu\Delta i_9 + \gamma_\nu k_\mu\Delta i_{11} + \gamma_\nu p_\mu\Delta i_{12}$$

$$+ \slashed{k}\frac{k_\mu k_\nu}{k \cdot p}\Delta i_{15} + \slashed{k}\frac{k_\mu p_\nu}{k \cdot p}\Delta i_{16} + \slashed{k}\frac{p_\mu k_\nu}{k \cdot p}\Delta i_{17}$$

$$+ \slashed{k}\frac{p_\mu p_\nu}{k \cdot p}\Delta i_{18} + \slashed{p}\frac{k_\mu k_\nu}{k \cdot p}\Delta i_{19} + \slashed{p}\frac{k_\mu p_\nu}{k \cdot p}\Delta i_{20}$$

$$\left. + \slashed{p}\frac{p_\mu k_\nu}{k \cdot p}\Delta i_{21} + \slashed{p}\frac{p_\mu p_\nu}{k \cdot p}\Delta i_{22}\right](1 - \gamma_5), \qquad (39)$$

$$\tilde{T}_{\mu\nu}^+(k, p) = aT_{\mu\nu}^+(k, p), \qquad (40)$$

$$\tilde{T}_{\mu\nu}^-(k, p) = T_{\mu\nu}^-(k, p) + \frac{\alpha_s}{4\pi}\left[\slashed{k}g_{\mu\nu}\frac{4}{3} - \slashed{p}g_{\mu\nu}\frac{4}{3} - \gamma_\mu k_\nu\frac{8}{3}\right.$$

$$\left. - \gamma_\mu p_\nu\frac{4}{3} + \gamma_\nu k_\mu\frac{4}{3} + \gamma_\nu p_\mu\frac{8}{3}\right](1 - \gamma_5), \qquad (41)$$

where the matrix E in Eq. (38) is defined by

$$E(\mu, \nu, k) = \gamma_\mu\gamma_\nu\slashed{k} - \gamma_\mu k_\nu + \gamma_\nu k_\mu - \slashed{k}g_{\mu\nu}$$

$$= -i\epsilon_{\mu\nu\alpha\beta}k^\alpha\gamma^\beta\gamma_5, \qquad (42)$$

with the second line obtained in a four dimension context with the Bjorken-Drell conventions. The parameter a in Eq. (40) denotes the chiral structure of the local four-quark operators in the weak interaction vertex with $a = \pm$ corresponding to $(V - A) \otimes (V \mp A)$, respectively. The

dimensionally regularized expressions for the Δi functions are collected in Appendix B.

Equipped with the explicit form for these building blocks, we can now evaluate all the Feynman diagrams in Fig. 6. After direct calculations, the final results with the subscript denoting the contraction of the corresponding operator in the weak interaction vertex are

$$\mathcal{A}_{Q_1} = i \frac{\alpha_s^2 f_B f_{M_1} f_{M_2}}{N_c^3} \lambda_p^{(l)} \int_0^1 d\xi \frac{\Phi_1^B(\xi)}{\xi} \int_0^1 dudv \left[-\frac{2}{3} - \frac{4}{3} \ln\frac{m_b}{\mu} + G(s_p, 1-u) \right] f_1(u, v)$$
$$+ i \frac{\alpha_s^2 f_B f_{M_1} f_{M_2}}{N_c^3} \lambda_p^{(l)} \int_0^1 d\xi \frac{\Phi_1^B(\xi)}{\xi} \int_0^1 dudv f_2(u, v, m_p), \tag{43}$$

$$\mathcal{A}_{Q_3} = -i \frac{\alpha_s^2 f_B f_{M_1} f_{M_2}}{N_c^3} \lambda_t^{(l)} \int_0^1 d\xi \frac{\Phi_1^B(\xi)}{\xi} \int_0^1 dudv \left[-\frac{4}{3} - \frac{8}{3} \ln\frac{m_b}{\mu} + G(0, 1-u) + G(1, 1-u) \right] f_1(u, v)$$
$$- i \frac{\alpha_s^2 f_B f_{M_1} f_{M_2}}{N_c^3} \lambda_t^{(l)} \int_0^1 d\xi \frac{\Phi_1^B(\xi)}{\xi} \int_0^1 dudv [f_2(u, v, 0) + f_2(u, v, m_b)], \tag{44}$$

$$\mathcal{A}_{Q_4} = -i \frac{\alpha_s^2 f_B f_{M_1} f_{M_2}}{N_c^3} \lambda_t^{(l)} \int_0^1 d\xi \frac{\Phi_1^B(\xi)}{\xi} \int_0^1 dudv \left[-\frac{4n_f}{3} \ln\frac{m_b}{\mu} + (n_f - 2)G(0, 1-u) + G(s_c, 1-u) + G(1, 1-u) \right]$$
$$\times f_1(u, v) - i \frac{\alpha_s^2 f_B f_{M_1} f_{M_2}}{N_c^3} \lambda_t^{(l)} \int_0^1 d\xi \frac{\Phi_1^B(\xi)}{\xi} \int_0^1 dudv [(n_f - 2)f_3(u, v, 0) + f_3(u, v, m_c) + f_3(u, v, m_b)], \tag{45}$$

$$\mathcal{A}_{Q_6} = -i \frac{\alpha_s^2 f_B f_{M_1} f_{M_2}}{N_c^3} \lambda_t^{(l)} \int_0^1 d\xi \frac{\Phi_1^B(\xi)}{\xi} \int_0^1 dudv \left[-\frac{4n_f}{3} \ln\frac{m_b}{\mu} + (n_f - 2)G(0, 1-u) + G(s_c, 1-u) + G(1, 1-u) \right]$$
$$\times f_1(u, v) - i \frac{\alpha_s^2 f_B f_{M_1} f_{M_2}}{N_c^3} \lambda_t^{(l)} \int_0^1 d\xi \frac{\Phi_1^B(\xi)}{\xi} \int_0^1 dudv [(n_f - 2)f_4(u, v, 0) + f_4(u, v, m_c) + f_4(u, v, m_b)], \tag{46}$$

with

$$f_1(u, v) = \Phi_{M_2}(u)\Phi_{M_1}(v) \left[\frac{1}{12(1-u)(1-v)} + \frac{3(3-2u-v)}{4(1-u)(1-v)v} \right]$$
$$+ r_\chi^{M_1} \Phi_{M_2}(u)\Phi_p^{M_1}(v) \left[\frac{3(3-v)}{4(1-u)(1-v)v} + \frac{2-u}{12(1-u)u(1-v)} \right]$$
$$- r_\chi^{M_1} r_\chi^{M_2} \Phi_p^{M_2}(u)\Phi_p^{M_1}(v) \left[\frac{1}{12(1-u)(1-v)} - \frac{3(3-2u-v+2uv)}{4(1-u)(1-v)v} \right]$$
$$+ r_\chi^{M_2} \Phi_p^{M_2}(u)\Phi_{M_1}(v) \left[\frac{1}{12(1-v)} + \frac{3(3-v)}{4(1-v)v} \right], \tag{47}$$

$$f_2(u, v, m_q) = \Phi_{M_2}(u)\Phi_{M_1}(v) \left[\frac{3\Delta i_2}{8(1-u)(1-v)} + \frac{3\Delta i_3}{8(1-u)v} + \frac{7\Delta i_6}{24(1-u)v} + \frac{3\Delta i_8}{8(1-v)v} + \frac{7\Delta i_{23}}{24(1-v)v} \right.$$
$$\left. + \frac{7(1-u+v)\Delta i_5}{24(1-u)(1-v)v} \right] - r_\chi^{M_1} \Phi_{M_2}(u)\Phi_p^{M_1}(v) \left[\frac{3}{8(1-u)v}(\Delta i_3 + \Delta i_{21}) + \frac{3\Delta i_{12}}{4(1-u)v} \right.$$
$$+ \frac{7}{24(1-u)v}(\Delta i_6 + \Delta i_{26}) + \frac{7\Delta i_5}{12(1-u)(1-v)} + \frac{3}{8(1-u)(1-v)}(\Delta i_2 - \Delta i_8 + \Delta i_{17}) \right]$$
$$- r_\chi^{M_2} \Phi_p^{M_2}(u)\Phi_{M_1}(v) \left[\frac{3\Delta i_2}{8(1-v)v} + \frac{7\Delta i_{23}}{24(1-v)v} + \frac{7\Delta i_5}{12(1-v)v} - \frac{3\Delta i_8}{8(1-v)} \right]$$
$$+ r_\chi^{M_1} r_\chi^{M_2} \Phi_p^{M_2}(u)\Phi_p^{M_1}(v) \left[\frac{7\Delta i_5}{12(1-v)} - \frac{3\Delta i_{12}}{8v} - \frac{7u\Delta i_{23}}{12(1-u)(1-v)} + \frac{3u}{8(1-u)v}(\Delta i_3 + \Delta i_{21}) \right.$$
$$\left. + \frac{7}{24(1-u)v}(\Delta i_6 + \Delta i_{26}) + \frac{3}{8}\left(\frac{1}{(1-u)(1-v)} + \frac{1}{v}\right)(\Delta i_2 + \Delta i_8 + \Delta i_{17}) \right], \tag{48}$$

$$
\begin{aligned}
f_{3,(4)}(u, v, m_q) = {}& \Phi_{M_2}(u)\Phi_{M_1}(v)\bigg[-\frac{(3 - 2u - 2v)}{2(1 - u)(1 - v)v} + \frac{3\Delta i_2}{8(1 - u)(1 - v)} + \frac{3\Delta i_3}{8(1 - u)v} \pm \frac{7(1 - u + v)\Delta i_5}{24(1 - u)(1 - v)v} \\
& \pm \frac{7\Delta i_6}{24(1 - u)v} + \frac{3\Delta i_8}{8(1 - v)v} \pm \frac{7\Delta i_{23}}{24(1 - v)v} \bigg] - r_\chi^{M_1}\Phi_{M_2}(u)\Phi_p^{M_1}(v)\bigg[\frac{3}{2(1 - u)(1 - v)v} \\
& + \frac{3}{8(1 - u)v}(\Delta i_3 + \Delta i_{21}) \pm \frac{7}{24(1 - u)v}(\Delta i_6 + \Delta i_{26}) + \frac{3\Delta i_{12}}{4(1 - u)v} \pm \frac{7\Delta i_5}{12(1 - u)(1 - v)} \\
& + \frac{3}{8(1 - u)(1 - v)}(\Delta i_2 - \Delta i_8 + \Delta i_{17}) \bigg] - r_\chi^{M_2}\Phi_p^{M_2}(u)\Phi_{M_1}(v)\bigg[\frac{3}{2(1 - v)v} + \frac{3\Delta i_2}{8(1 - v)v} \\
& \pm \frac{7\Delta i_{23}}{24(1 - v)v} \pm \frac{7\Delta i_5}{12(1 - v)v} - \frac{3\Delta i_8}{8(1 - v)} \bigg] + r_\chi^{M_1}r_\chi^{M_2}\Phi_p^{M_2}(u)\Phi_p^{M_1}(v)\bigg[-\frac{3 - 2u - 2v + 2uv}{2(1 - u)(1 - v)v} \\
& \pm \frac{7\Delta i_5}{12(1 - v)} - \frac{3\Delta i_{12}}{8v} \mp \frac{7u\Delta i_{23}}{12(1 - u)(1 - v)} + \frac{3u}{8(1 - u)v}(\Delta i_3 + \Delta i_{21}) \pm \frac{7}{24(1 - u)v}(\Delta i_6 + \Delta i_{26}) \\
& + \frac{3}{8}\bigg(\frac{1}{(1 - u)(1 - v)} + \frac{1}{v}\bigg)(\Delta i_2 + \Delta i_8 + \Delta i_{17}) \bigg],
\end{aligned}
\tag{49}
$$

where the argument m_q is the quark mass propagating in the fermion loops. At this stage, the Δ_i functions are the ones that have been performed with the Feynman parameter integrals, whose explicit forms can be found in Appendix B.

With the individual operator contributions given above, the total contributions of these higher order $b \to Dg^*g^*$ strong penguin diagrams to the decay amplitudes of $B \to M_1M_1$ modes can be written as

$$
\begin{aligned}
\mathcal{A}_{b \to Dg^*g^*} = \frac{G_F}{\sqrt{2}}\big[& C_{8g}^{\text{eff}}\mathcal{A}_{Q_{8g}} + C_1\mathcal{A}_{Q_1} + C_3\mathcal{A}_{Q_3} \\
& + C_4\mathcal{A}_{Q_4} + C_6\mathcal{A}_{Q_6}\big].
\end{aligned}
\tag{50}
$$

In order to specialize these general results to $B \to \pi K$, $\pi\pi$ decays, we just need to replace M_1 and M_2 with the corresponding mesons. Explicitly, the $b \to Dg^*g^*$ strong penguin contributions to the decay amplitudes of the four $B \to \pi K$ and the three $B \to \pi\pi$ decay channels are

$$
\begin{aligned}
\mathcal{A}'(B^- \to \pi^-\overline{K}^0) = {}& \mathcal{A}'(\overline{B}^0 \to \pi^+K^-) \\
& = \mathcal{A}_{b \to sg^*g^*}(M_1 \to \pi, M_2 \to K), \\
\sqrt{2}\mathcal{A}'(B^- \to \pi^0K^-) = {}& -\sqrt{2}\mathcal{A}'(\overline{B}^0 \to \pi^0\overline{K}^0) \\
& = \mathcal{A}_{b \to sg^*g^*}(M_1 \to \pi, M_2 \to K),
\end{aligned}
\tag{51}
$$

$$
\begin{aligned}
\mathcal{A}'(\overline{B}^0 \to \pi^+\pi^-) = {}& \mathcal{A}'(\overline{B}^0 \to \pi^0\pi^0) \\
& = \mathcal{A}_{b \to dg^*g^*}(M_1 \to \pi, M_2 \to \pi), \\
\mathcal{A}'(B^- \to \pi^-\pi^0) = {}& 0,
\end{aligned}
\tag{52}
$$

where the superscript "$\prime$" is indicated there to be distinguished from the next-to-leading order results given by Eqs. (18) and (19). The total decay amplitudes are then the sum of these two pieces.

With the total decay amplitudes, the branching ratio for $B \to M_1M_2$ decays reads

$$
\begin{aligned}
\mathcal{B}(B \to M_1M_2) = \frac{\tau_B p_c}{8\pi m_B^2}|\mathcal{A}(B \to M_1M_2) \\
+ \mathcal{A}'(B \to M_1M_2)|^2 \cdot S,
\end{aligned}
\tag{53}
$$

where τ_B is the lifetime of the B meson, $S = 1/2$ if M_1 and M_2 are identical, and $S = 1$ otherwise. p_c is the magnitude of the momentum of the final-state particle $M_{1,2}$ in the B-meson rest frame and is given by

$$
p_c = \frac{1}{2m_B}\sqrt{[m_B^2 - (m_{M_1} + m_{M_2})^2][m_B^2 - (m_{M_1} - m_{M_2})^2]}.
\tag{54}
$$

As for the direct CP asymmetries, we use the definition of the difference of the $\bar{B}$-meson minus B-meson decay rates divided by their sum. With the branching ratios of the CP-conjugated modes denoted by $\mathcal{B}(\bar{B} \to \bar{f})$, the CP-averaged branching ratios and the direct CP asymmetries for $B \to f$ decays can be expressed, respectively, as

$$
\bar{\mathcal{B}} = \frac{1}{2}[\mathcal{B}(\bar{B} \to \bar{f}) + \mathcal{B}(B \to f)],
\tag{55}
$$

$$
\mathcal{A}_{CP} = \frac{\mathcal{B}(\bar{B} \to \bar{f}) - \mathcal{B}(B \to f)}{\mathcal{B}(\bar{B} \to \bar{f}) + \mathcal{B}(B \to f)}.
\tag{56}
$$

III. NUMERICAL CALCULATION AND DISCUSSIONS

A. Input parameters

The theoretical predictions with the QCDF approach depend on many input parameters such as the CKM matrix elements, Wilson coefficients, hadronic parameters, and so on. We present all the relevant input parameters as follows.

Wilson coefficients.—The Wilson coefficients $C_i(\mu)$ in the effective weak Hamiltonian have been reliably evaluated to the next-to-leading logarithmic order. To proceed, we use the following numerical values at the $\mu = m_b$ scale, which have been obtained in the NDR scheme [49,58],

$$
\begin{aligned}
&C_1 = 1.082, \quad\quad C_2 = -0.185, \quad\quad C_3 = 0.014, \\
&C_4 = -0.035, \quad\quad C_5 = 0.009, \quad\quad C_6 = -0.041, \\
&\quad\quad C_7/\alpha = -0.011, \quad\quad C_8/\alpha = 0.059, \\
&\quad\quad C_9/\alpha = -1.241, \quad\quad C_{10}/\alpha = 0.218, \\
&\quad\quad C_{7\gamma}^{\text{eff}} = -0.299, \quad\quad C_{8g}^{\text{eff}} = -0.143.
\end{aligned}
\tag{57}
$$

The CKM matrix elements.—The widely used parametrization of the CKM matrix elements in analyzing B-meson decays is the Wolfenstein parametrization, which emphasizes the hierarchies among its elements and is expanded as a power series in the parameter $\lambda = |V_{us}|$ [59],

$$
V_{\text{CKM}} = \begin{pmatrix} 1 - \frac{\lambda^2}{2} & \lambda & A\lambda^3(\rho - i\eta) \\ -\lambda & 1 - \frac{\lambda^2}{2} & A\lambda^2 \\ A\lambda^3(1 - \rho - i\eta) & -A\lambda^2 & 1 \end{pmatrix}
$$
$$
+ \mathcal{O}(\lambda^4).
\tag{58}
$$

The values of the four Wolfenstein parameters (A, λ, ρ, and η) could be determined from the best knowledge of the experimental and theoretical inputs. In this paper, we take

$$
\begin{aligned}
&A = 0.8533, \quad\quad \lambda = 0.2200, \\
&\bar{\rho} = 0.20, \quad\quad \bar{\eta} = 0.33,
\end{aligned}
\tag{59}
$$

as our default input values [60]. The parameters $\bar{\rho}$ and $\bar{\eta}$ are defined by $\bar{\rho} = \rho(1 - \frac{\lambda^2}{2})$, $\bar{\eta} = \eta(1 - \frac{\lambda^2}{2})$.

Masses and lifetimes.—For the quark mass, there are two different classes appearing in the QCDF approach. One type is the pole quark mass which appears in the evaluation of the penguin loop corrections, and is denoted by m_q with $q = u, d, s, c, b$. In this paper, we take

$$
\begin{aligned}
m_u = m_d = m_s = 0, \quad\quad m_c = 1.47 \text{ GeV}, \\
m_b = 4.80 \text{ GeV},
\end{aligned}
\tag{60}
$$

as our default input values.

The other one is the current quark mass which appears in the equations of motion and is used to calculate the matrix elements of the penguin operators as well as the chiral enhancement factors r_χ^M. This kind of quark mass is scale dependent. To get the corresponding value at the given scale, we should use the renormalization group equation to run them, which can be found, for example, in [49]. Following Ref. [25], we hold $(\bar{m}_u + \bar{m}_d)/\bar{m}_s$ fixed and use $\bar{m}_s$ as an input parameter. Explicitly, we take

$$
\begin{aligned}
\bar{m}_u(2 \text{ GeV}) = \bar{m}_d(2 \text{ GeV}) = 0.0413\bar{m}_s(2 \text{ GeV}), \\
\bar{m}_s(2 \text{ GeV}) = 90 \text{ MeV}, \quad\quad \bar{m}_b(m_b) = 4.40 \text{ GeV},
\end{aligned}
\tag{61}
$$

where the difference between the u and d quark is not distinguished.

For meson masses and the lifetimes of the B meson, we adopt the center values given by [60]

$$
\tau_{B_u} = 1.671 \text{ ps}, \quad \tau_{B_d} = 1.536 \text{ ps}, \quad m_{B_u} = 5.2794 \text{ GeV}, \quad m_{B_d} = 5.2790 \text{ GeV},
$$
$$
m_{K^\pm} = 493.7 \text{ MeV}, \quad m_{K^0} = 497.6 \text{ MeV}, \quad m_{\pi^\pm} = 139.6 \text{ MeV}, \quad m_{\pi^0} = 135.0 \text{ MeV}.
$$

Light-cone distribution amplitudes of mesons.—Since the QCDF approach is based on the heavy-quark assumption, to a very good approximation, we can use the asymptotic form of the LCDAs for light mesons [53,56,61]

$$
\Phi_M(x) = 6x(1 - x), \quad\quad \Phi_p^M(x) = 1.
\tag{62}
$$

With respect to the endpoint divergence associated with the momentum fraction integral over the LCDAs appearing in this paper, in analogy to the treatment in Refs. [21,62], we regulate the integral with an *ad hoc* cutoff

$$
\int_0^1 dv \frac{\Phi_p^M(v)}{1 - v} \to \int_0^{1-\Lambda_h/m_B} dv \frac{\Phi_p^M(v)}{1 - v} = \ln\frac{m_B}{\Lambda_h},
\tag{63}
$$

with $\Lambda_h = 500$ MeV, and do not distinguish whether this divergence comes from the hard spectator rescattering or from the annihilation contributions. The possible complex phase associated with this integral has also been neglected.

As for the B-meson wave functions, within our approximation, we need only consider the first inverse moment of the LCDA $\Phi_1^B(\xi)$ defined by [21]

$$
\int_0^1 \frac{d\xi}{\xi} \Phi_1^B(\xi) \equiv \frac{m_B}{\lambda_B},
\tag{64}
$$

where the hadronic parameter λ_B has been introduced to parametrize this integral. This parameter has been evaluated using different methods [63,64] recently. In this paper, we take $\lambda_B = 460$ MeV as our default input value [63].

Decay constants and transition form factors.—The decay constants and the form factors are nonperturbative parameters and can be determined from experiments and/ or theoretical estimations. For the decay constants, we take

$$
f_B = 200 \text{ MeV}.
\tag{65}
$$

For the form factors involving the $B \to K$ and $B \to \pi$ transitions, we take

$$F_0^{B\to\pi}(0) = 0.258, \qquad F_0^{B\to K}(0) = 0.331, \qquad (66)$$

as the default values at the maximum recoil. In addition, we use the formula

$$F_0^{B\to M}(q^2) = \frac{r_2^M}{1 - q^2/m_{fit}^2(M)}, \qquad (67)$$

to parametrize the dependence of this form factor on the momentum-transfer q^2, with the fit parameters given by

$$
\begin{aligned}
r_2^\pi &= 0.258, & m_{fit}^2(\pi) &= 33.81, \\
r_2^K &= 0.330, & m_{fit}^2(K) &= 37.46.
\end{aligned}
\qquad (68)
$$

All of these values are taken from the latest QCD sum rule analysis [65].

B. Numerical results and discussions

With the theoretical expressions and the input parameters given above, we can now evaluate the branching ratios and the direct CP asymmetries for $B \to \pi K$ and $B \to \pi\pi$ decays. For each quantity, we first give the predictions at the next-to-leading order in α_s, and then take into account the $b \to Dg^*g^*$ strong penguin corrections, which are of order α_s^2. The combining contributions of the two pieces, denoted by $\mathcal{O}(\alpha_s + \alpha_s^2)$, are then given in the last. For comparison, the NF results are also presented. All the averaged experimental data are taken from HFAG [28].

1. The CP-averaged branching ratios for $B \to \pi K$, $\pi\pi$ decays

In the SM, the four $B \to \pi K$ decays are dominated by the $b \to s$ strong penguin diagrams, with additional subdominant contributions from the tree and electroweak penguin diagrams. The three $B \to \pi\pi$ decays, however, are tree-dominated modes. It is therefore expected that these

higher order strong penguin diagrams considered in this paper should contribute effectively to $B \to \pi K$ modes, while having only a minor impact on $B \to \pi\pi$ ones. Numerical results of the CP-averaged branching ratios for these modes are collected in Table I.

The dependence of these CP-averaged branching ratios on the weak phase γ is shown by Fig. 9 (without the annihilation contributions) and Fig. 10 (with the annihilation contributions), where the solid and dashed lines correspond to the theoretical predictions with and without the $b \to Dg^*g^*$ strong penguin contributions included, respectively. The horizontal solid lines denote the experimental data as given in Table I, with the thicker one denoting its center value and the thinner ones its error bars. In these and the following figures, the default values of all inputs parameters except for the CKM angle γ are used.

From these two figures and the numerical results given by Table I, we can see that:

(i) For penguin-dominated $B \to \pi K$ decays, due to the enhancement of the penguin amplitudes, the QCDF scheme prefers larger branching ratios than the NF approximation. With our default input parameters, however, predictions for the branching rations are still smaller than the experimental data even after the inclusion of the annihilation contributions, if we consider only contributions up to the next-to-leading order in α_s. The effects of these higher order $b \to sg^*g^*$ strong penguin corrections are very prominent in these penguin-dominated $B \to \pi K$ decays. With our input parameters, we find that these higher order strong penguin contributions can give $\sim 30\%$ enhancement to the corresponding branching ratios, and such an enhancement can improve the consistency between the theoretical predictions and the experimental data significantly. In addition, we find that the effect of the annihilation contributions on the branching ratios, though not negligible, is not so large as claimed by the pQCD method [2,51].

TABLE I. The CP-averaged branching ratios (in units of 10^{-6}) for $B \to \pi K$, $\pi\pi$ decays with the default input parameters. $\bar{\mathcal{B}}^f$ and $\bar{\mathcal{B}}^{f+a}$ denote the results without and with the annihilation contributions, respectively. The NF results, which are of order $\mathcal{O}(\alpha_s^0)$, are also shown for comparison. $\bar{\rho} = 0.20$ and $\bar{\eta} = 0.33$.

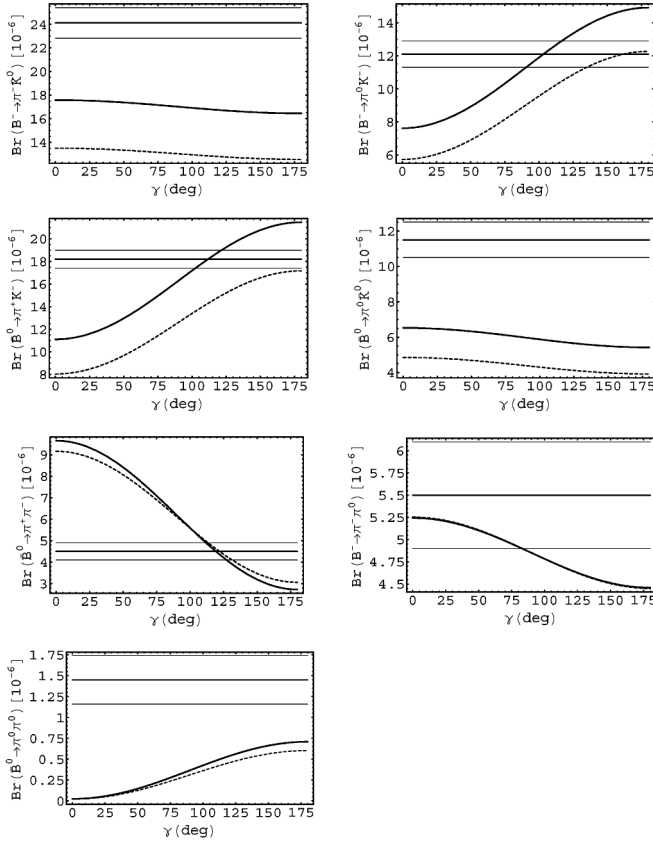| Decay mode	NF	$\bar{\mathcal{B}}^f$		$\bar{\mathcal{B}}^{f+a}$		Exp.
		$\mathcal{O}(\alpha_s)$	$\mathcal{O}(\alpha_s + \alpha_s^2)$	$\mathcal{O}(\alpha_s)$	$\mathcal{O}(\alpha_s + \alpha_s^2)$	
$B^- \to \pi^- \overline{K}^0$	10.07	13.28	17.31	16.04	20.44	24.1 ± 1.3
$B^- \to \pi^0 K^-$	5.69	7.30	9.37	8.72	10.97	12.1 ± 0.8
$\overline{B}^0 \to \pi^+ K^-$	7.71	10.25	13.61	12.46	16.15	18.2 ± 0.8
$\overline{B}^0 \to \pi^0 \overline{K}^0$	3.38	4.63	6.26	5.70	7.50	11.5 ± 1.0
$\overline{B}^0 \to \pi^+ \pi^-$	7.41	7.69	7.99	8.32	8.63	4.5 ± 0.4
$B^- \to \pi^- \pi^0$	5.12	5.06	5.06	$\cdots$	$\cdots$	5.5 ± 0.6
$\overline{B}^0 \to \pi^0 \pi^0$	0.15	0.16	0.19	0.17	0.21	1.45 ± 0.29

FIG. 9. The γ dependence of the *CP*-averaged branching ratios for $B \to \pi K, \pi\pi$ decays without the annihilation contributions. The solid and dashed lines correspond to the theoretical predictions with and without the $b \to Dg^*g^*$ strong penguin contributions included, respectively. The horizontal solid lines denote the experimental data as given in Table I, with the thicker ones being its center values and the thinner its error bars.

FIG. 10. The γ dependence of the *CP*-averaged branching ratios for $B \to \pi K, \pi\pi$ decays with the annihilation contributions included. The meaning of the curves and the horizontal solid lines is the same as in Fig. 9.

(ii) For tree-dominated $B \to \pi\pi$ decays, the higher order $b \to dg^*g^*$ contributions play only a minor role. To a very good approximation, the $B^\pm \to \pi^\pm\pi^0$ decay can be considered as a pure tree process, and it does not receive annihilation contributions either. The theoretical prediction for the corresponding branching ratio agrees with the data quite well. For the other two $B \to \pi\pi$ modes, however, theoretical predictions with QCDF approach are quite inconsistent with the measured ratios, even with the annihilation and the higher order strong penguin contributions included. With our input parameters, we find that the theoretical prediction for the $\bar{B}^0 \to \pi^0\pi^0$ mode is about an eighth of the experimental data; for the $\bar{B}^0 \to \pi^+\pi^-$ mode, on the other hand, a value about 2 times larger than the data is predicted.

(iii) As for the γ dependence of the corresponding branching ratios, we can see that the two decay modes, $B^\pm \to \pi^\pm\pi^0$ and $B^\pm \to \pi^\pm K^0$, are almost independent of this angle, since the corresponding

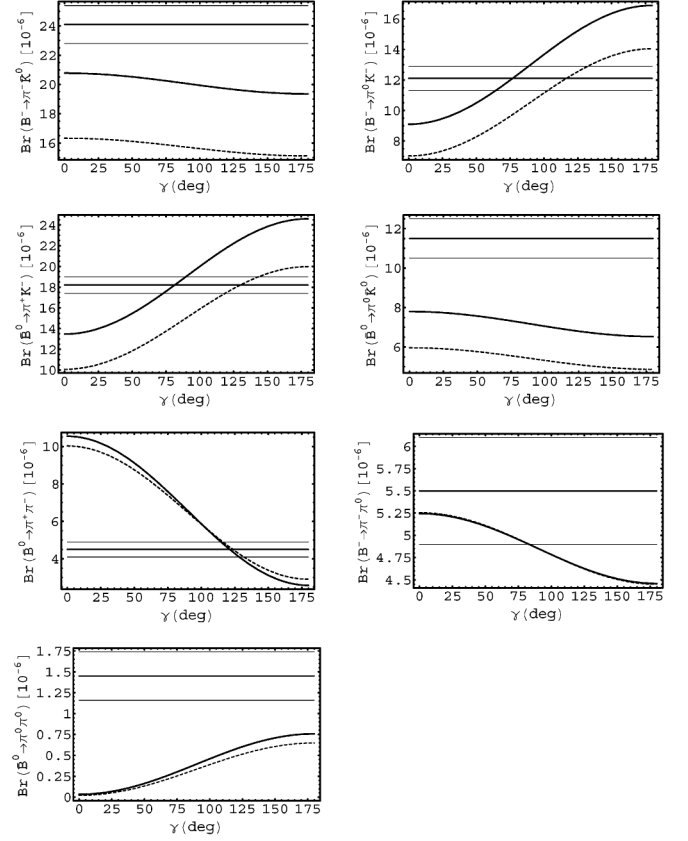decay amplitudes have to a good approximation only a single weak phase. In addition, the discrepancy between the theoretical prediction and the experimental data for $\bar{B}^0 \to \pi^+\pi^-$ can be removed if we use a large angle $\gamma \sim 120°$. With the annihilation and the higher order strong penguin contributions included, the four $B \to \pi K$ modes, however, prefer a smaller value for this angle around $\gamma \sim 80°$, which is quite consistent with the latest direct experimental measurement $\gamma = 81° \pm 19°(\text{stat.}) \pm 13°(\text{sys.}) \pm 11°(\text{model})$ [66].

(iv) The theoretical predictions for the branching ratios are very sensitive to the value of the form factor $F_0^{B\to\pi}$. For example, the large measured decay rates for the four $B \to \pi K$ decays can be well accommodated with a larger value of the form factor as shown by Beneke and Neubert [25]. On the other hand, the prediction for $\bar{B}^0 \to \pi^+\pi^-$ decays can become consistent with the data only when a smaller value is used. The large measured ratio for $\bar{B}^0 \to \pi^0\pi^0$, however, remains unresolved with the varying of these parameters. It is a tough theoretical challenge to accommodate the current experimental data in the SM.

TABLE II. Ratios between the *CP*-averaged branching fractions for $B \to \pi K, \pi\pi$ modes. The values in the parentheses are the ones without the annihilation contributions.

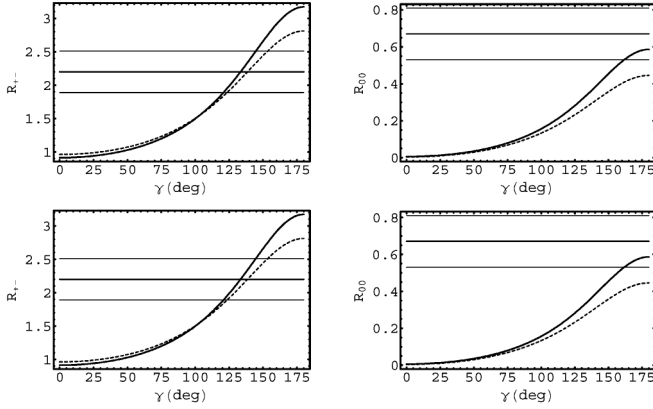|	NF	$\mathcal{O}(\alpha_s)$	$\mathcal{O}(\alpha_s + \alpha_s^2)$	Exp.
R_{+-}	1.272	1.119 (1.209)	1.077 (1.163)	2.20 ± 0.31
R_{00}	0.040	0.041 (0.042)	0.048 (0.047)	0.67 ± 0.14
R	0.833	0.845 (0.840)	0.860 (0.855)	0.82 ± 0.06
R_c	1.130	1.087 (1.100)	1.074 (1.083)	1.00 ± 0.09
R_n	1.140	1.092 (1.106)	1.077 (1.087)	0.79 ± 0.08

FIG. 11. Ratios of the *CP*-averaged branching fractions defined by Eq. (2) as functions of the weak phase γ. The meaning of the curves and the horizontal solid lines is the same as in Fig. 9.

Since the uncertainties in the predictions for branching ratios can be largely eliminated by taking ratios between them, we now discuss the variations of the quantities defined by Eq. (2) with the higher order $b \to Dg^*g^*$ strong penguin contributions included. It is the known "πK" puzzle [29,30] that the SM predictions are inconsistent with current experiment data. The theoretical predictions and the current experimental data for these ratios are collected in Table II. For the γ dependence of these quantities, we display them in Fig. 11, where the curves and the

horizontal solid lines have the same interpretations as in Fig. 9.

From Table II and Fig. 11, we can find that the two ratios R_c and R_n are indeed approximately equal within the SM as claimed in Ref. [30], while the experimental data for the two quantities are quite different with the puzzling pattern $R_n < 1$. On the other hand, the value of the quantity R predicted by the QCDF approach is well consistent with the experimental data. For the other two ratios R_{+-} and R_{00}, the discrepancies between the theoretical predictions and the experimental data are quite large. As the $b \to Dg^*g^*$ strong penguin contributions to $B \to \pi K, \pi\pi$ decays are similar in nature, and hence eliminated in the ratios between the corresponding branching fractions, the patterns of the these quantities remain unaffected even with these new strong penguin contributions included. From the γ dependence of the ratios between the four $B \to \pi K$ decays, a smaller value for this phase is preferred. On the other hand, a larger value for this phase is favored by $B \to \pi\pi$ decays. These inconsistencies may be hints for new physics playing in the electroweak penguin sector as suggested by Buras *et al.* [30].

2. The direct *CP* asymmetries for $B \to \pi K, \pi\pi$ decays

Contrary to the NF approximation, the QCDF scheme can predict the strong-interaction phases and hence the direct *CP* asymmetries in the heavy-quark limit. The numerical results and the experimental data for this quantity involving the four πK and the three $\pi\pi$ final states are collected in Table III. The γ dependence of the direct *CP* asymmetries is displayed in Fig. 12 (without the annihilation contributions) and Fig. 13 (with the annihilation contributions), in which the curves and the horizontal solid lines also have the same interpretation as in Fig. 9.

From these two figures and the numerical results given in Table III, we can see that:
  (i) The direct *CP* asymmetries for $B \to \pi K, \pi\pi$ decays are predicted to be typically small with the QCDF formalism. This could be well understood,

TABLE III. The direct *CP* asymmetries (in units of 10^{-2}) for $B \to \pi K, \pi\pi$ decays with the default input parameters. A_{CP}^f and A_{CP}^{f+a} denote the results without and with the annihilation contributions, respectively.

Decay mode	A_{CP}^f		A_{CP}^{f+a}		Exp.
	$\mathcal{O}(\alpha_s)$	$\mathcal{O}(\alpha_s + \alpha_s^2)$	$\mathcal{O}(\alpha_s)$	$\mathcal{O}(\alpha_s + \alpha_s^2)$	
$B^- \to \pi^- \overline{K}^0$	0.73	0.52	0.65	0.46	-2.0 ± 3.4
$B^- \to \pi^0 K^-$	7.59	6.94	6.56	6.07	4 ± 4
$\overline{B}^0 \to \pi^+ K^-$	5.31	4.83	4.39	4.08	-10.9 ± 1.9
$\overline{B}^0 \to \pi^0 \overline{K}^0$	-3.08	-2.84	-2.71	-2.54	-9 ± 14
$\overline{B}^0 \to \pi^+ \pi^-$	-4.73	-5.51	-4.54	-5.27	37 ± 10
$B^- \to \pi^- \pi^0$	-0.30	-0.31	$\cdots$	$\cdots$	-2 ± 7
$\overline{B}^0 \to \pi^0 \pi^0$	55.52	58.53	55.03	55.50	28 ± 39

FIG. 12.   The γ dependence of the *CP* asymmetries without the annihilation contributions. The meaning of the curves and the horizontal solid lines is the same as in Fig. 9.
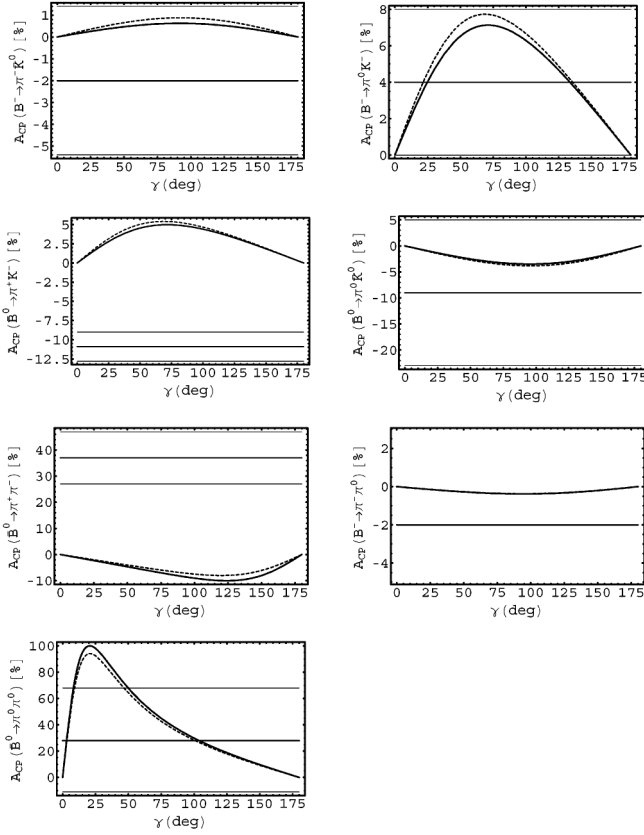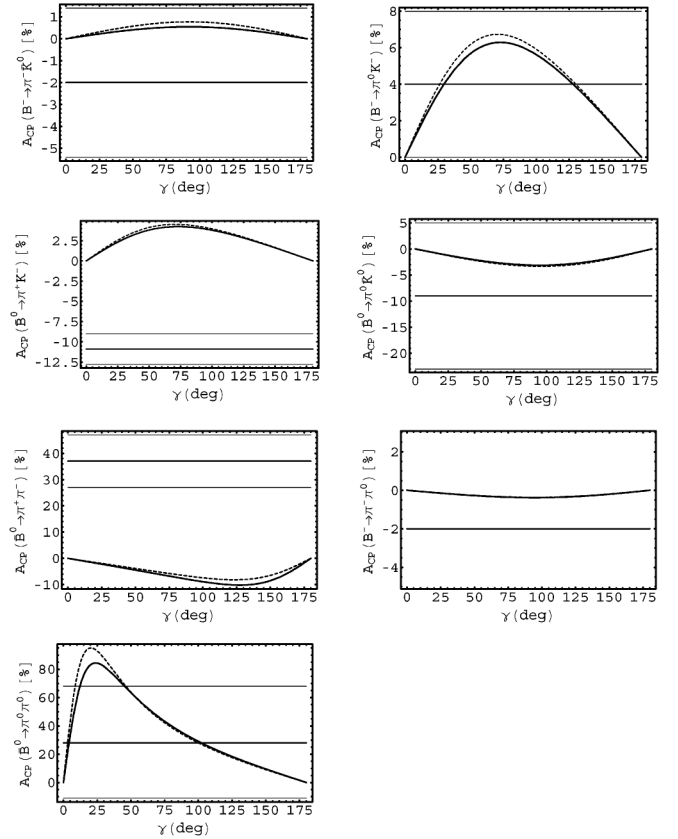

FIG. 13.   The γ dependence of the *CP* asymmetries with the annihilation contributions included. The meaning of the curves and the horizontal solid lines is the same as in Fig. 9.

since the direct *CP* asymmetries are proportional to the sines of the strong-interaction phases, which are usually suppressed by α_s and/or $\Lambda_{\mathrm{QCD}}/m_b$ within the QCDF formalism. Because of a potentially large relative phase between the QCD penguins and the coefficient a_2, the $\overline{B}^0 \to \pi^0 \pi^0$ mode, however, is an exception to this general rule. The direct *CP* asymmetries for this mode is predicted to be about 55%.

(ii) Although the individual Feynman diagram in Fig. 6 carries a large strong phase, the combining contributions of these $b \to Dg^*g^*$ strong penguin diagrams contain only a relatively small one. Thus, these higher order strong penguin contributions to the direct *CP* asymmetries are also small.

(iii) The theoretical predictions for $A_{CP}(\overline{B}^0 \to \pi^+ \pi^-)$ and $A_{CP}(\overline{B}^0 \to \pi^+ K^-)$ are quite smaller than the experimental data, particularly with the opposite sign. How to accommodate these discrepancies in the SM is still a challenge.

IV. CONCLUSIONS

In this paper, we have revisited the $B \to \pi K$, $\pi\pi$ decays in the framework of QCDF with the $b \to Dg^*g^*$ strong penguin contributions included. The main conclusions of this paper are:

(1) For penguin-dominated $B \to \pi K$ decays, the higher order strong penguin contributions induced by $b \to sg^*g^*$ transitions to the branching ratios are rather large. With our input parameters, we find that these higher order strong penguin contributions can give $\sim 30\%$ enhancement to the corresponding branching ratios, and such an enhancement can improve the consistency between the theoretical predictions and the experimental data significantly.

(2) For tree-dominated $B \to \pi\pi$ decays, the higher order $b \to dg^*g^*$ contributions to the corresponding branching ratios are quite small.

(3) Because of large cancellations among the $b \to Dg^*g^*$ strong penguin contributions, only a relatively small strong phase remains, so that the contributions have small effects on predictions of the direct *CP* asymmetries.

(4) Since corrections of these higher order strong penguin diagrams to the decay amplitudes are similar in nature, and hence canceled in the ratios between the corresponding branching fractions, the patterns of the quantities R, R_c, R_n, R_{+-}, and R_{00} remain unaffected compared to the next-to-leading order re-

sults. So we have not found a solution to the "πK" puzzle. Our results indicate that to resolve the puzzle we may have to resort to new physics contributions through the electroweak penguin sector as observed by Buras *et al.* [30].

(5) The theoretical predictions for the branching ratios and the direct *CP* asymmetries still have large theoretical uncertainties. The dominant errors are induced by the uncertainties of the $F_0^{B\to\pi,K}(q^2)$ form factors, strange quark mass $\overline{m}_s(\mu)$, and the CKM angle γ.

Although the results presented here still have large theoretical uncertainties, the $b \to Dg^*g^*$ strong penguin contributions to two-body hadronic *B*-meson decays, particularly to penguin-dominated modes, have been shown to be very important. Further systematic studies on these higher order contributions to charmless *B* decays are therefore interesting and deserving.

ACKNOWLEDGMENTS

Note added.—After this work was finished, we note an interesting study of α_s^2 corrections to $B \to \pi K$, $\pi\pi$ decays has been carried out by Li, Mishima, and Sanda [67] in pQCD formalism. However, the contributions studied here as depicted by the Feynman diagrams in Figs. 5 and 6 are not included in their paper.

APPENDIX A: CORRECTION FUNCTIONS AT NEXT-TO-LEADING ORDER IN α_s

In this appendix, we present the explicit form for the correction functions appearing in the parameters a_i and b_i. Details about the calculation can be found in Refs. [21,25].

One-loop vertex corrections.—The vertex parameters $V_i(M_2)$ result from the first four diagrams in Fig. 2, given by (with $M_2 = \pi$, or K)

$$V_i(M_2) = \begin{cases} \int_0^1 du\,\Phi_{M_2}(u)[12\ln\frac{m_b}{\mu} - 18 + g(u)] & i = 1\text{–}4, 9, 10, \\ \int_0^1 du\,\Phi_{M_2}(u)[-12\ln\frac{m_b}{\mu} + 6 - g(1-u)] & i = 5, 7, \\ \int_0^1 du\,\Phi_p^{M_2}(u)[-6] & i = 6, 8, \end{cases} \tag{A1}$$

with

$$g(u) = 3\left[\frac{1-2u}{1-u}\ln u - i\pi\right]. \tag{A2}$$

The scheme-dependent constants -18, 6, -6 are specific to the NDR scheme for γ_5. Φ_{M_2} and $\Phi_p^{M_2}$ denote the leading-twist and twist-3 LCDAs of the emitted meson M_2, respectively.

Penguin contractions.—The QCD and electroweak penguin parameters $P_{4,6}^p$ and $P_{8,10}^p$ arise from the diagrams in Figs. 2(e) and 2(f). Considering the fact that there exist two distinct penguin contractions as shown in Fig. 14, these penguin contributions can be written as

$$P_4^p(M_2) = \frac{C_F\alpha_s}{4\pi N_c}\left\{C_1\left[\frac{4}{3}\ln\frac{m_b}{\mu} + \frac{2}{3} - G_{M_2}(s_p)\right]\right.$$
$$+ C_3\left[\frac{8}{3}\ln\frac{m_b}{\mu} + \frac{4}{3} - G_{M_2}(0) - G_{M_2}(1)\right]$$
$$+ (C_4 + C_6)\left[\frac{4n_f}{3}\ln\frac{m_b}{\mu} - (n_f - 2)G_{M_2}(0)\right.$$
$$\left. - G_{M_2}(s_c) - G_{M_2}(1)\right]$$
$$\left. - 2C_{8g}^{\text{eff}}\int_0^1 \frac{du}{1-u}\Phi_{M_2}(u)\right\}, \tag{A3}$$

$$P_6^p(M_2) = \frac{C_F\alpha_s}{4\pi N_c}\left\{C_1\left[\frac{4}{3}\ln\frac{m_b}{\mu} + \frac{2}{3} - \hat{G}_{M_2}(s_p)\right]\right.$$
$$+ C_3\left[\frac{8}{3}\ln\frac{m_b}{\mu} + \frac{4}{3} - \hat{G}_{M_2}(0) - \hat{G}_{M_2}(1)\right]$$
$$+ (C_4 + C_6)\left[\frac{4n_f}{3}\ln\frac{m_b}{\mu} - (n_f - 2)\hat{G}_{M_2}(0)\right.$$
$$\left. - \hat{G}_{M_2}(s_c) - \hat{G}_{M_2}(1)\right] - 2C_{8g}^{\text{eff}}\right\}, \tag{A4}$$

$$P_{10}^p(M_2) = \frac{\alpha}{9\pi N_c}\left\{(C_1 + N_c C_2)\left[\frac{4}{3}\ln\frac{m_b}{\mu} + \frac{2}{3} - G_{M_2}(s_p)\right]\right.$$
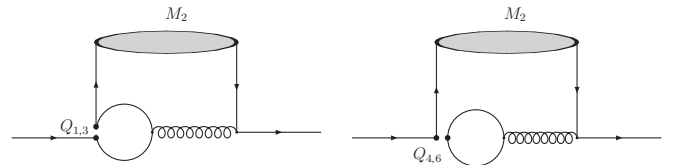$$\left. - 3C_{7\gamma}^{\text{eff}}\int_0^1 \frac{du}{1-u}\Phi_{M_2}(u)\right\}, \tag{A5}$$

FIG. 14. Two different penguin contractions.

$$P_8^p(M_2) = \frac{\alpha}{9\pi N_c}\left\{(C_1 + N_c C_2)\left[\frac{4}{3}\ln\frac{m_b}{\mu} + \frac{2}{3} - \hat{G}_{M_2}(s_p)\right]\right.$$
$$\left. - 3C_{7\gamma}^{\text{eff}}\right\}, \tag{A6}$$

where $C_F = (N_c^2 - 1)/2N_c$, and $N_c = 3$ is the number of colors. $n_f = 5$ is the number of light-quark flavors. The pole quark mass ratios, $s_u = 0$, $s_c = (m_c/m_b)^2$, are involved in the evaluation of these penguin diagrams. The functions $G_{M_2}(s)$ and $\hat{G}_{M_2}(s)$ are defined, respectively, by

$$G_{M_2}(s) = \int_0^1 du\, G(s, 1 - u)\Phi_{M_2}(u),$$
$$\hat{G}_{M_2}(s) = \int_0^1 du\, G(s, 1 - u)\Phi_p^{M_2}(u), \tag{A7}$$

with

$$G(s, u) = -4\int_0^1 dx\, x(1 - x)\ln[s - x(1 - x)u - i\delta], \tag{A8}$$

where the term $i\delta$ is the "ϵ prescription." The interpretation of Φ_{M_2} and $\Phi_p^{M_2}$ is the same as in the discussion of vertex corrections.

Hard spectator interactions.—The parameters $H_i(M_1 M_2)$ originate from the hard gluon exchange between the meson M_2 and the spectator quark (corresponding to the last two diagrams in Fig. 2) with the results given by

$$H_i(M_1 M_2) = \frac{f_B f_{M_1}}{(m_B^2 - m_{M_1}^2)F_0^{B\to M_1}(m_{M_2}^2)}\int_0^1 \frac{d\xi}{\xi}\Phi_1^B(\xi)$$
$$\times \int_0^1 du \int_0^1 dv \left[\frac{\Phi_{M_2}(u)\Phi_{M_1}(v)}{(1 - u)(1 - v)}\right.$$
$$\left. + r_\chi^{M_1}\frac{\Phi_{M_2}(u)\Phi_p^{M_1}(v)}{u(1 - v)}\right], \tag{A9}$$

for $i = 1$–$4, 9, 10$,

$$H_i(M_1 M_2) = -\frac{f_B f_{M_1}}{(m_B^2 - m_{M_1}^2)F_0^{B\to M_1}(m_{M_2}^2)}\int_0^1 \frac{d\xi}{\xi}\Phi_1^B(\xi)$$
$$\times \int_0^1 du \int_0^1 dv \left[\frac{\Phi_{M_2}(u)\Phi_{M_1}(v)}{u(1 - v)}\right.$$
$$\left. + r_\chi^{M_1}\frac{\Phi_{M_2}(u)\Phi_p^{M_1}(v)}{(1 - u)(1 - v)}\right], \tag{A10}$$

for $i = 5, 7$, and $H_i(M_1 M_2) = 0$ for $i = 6, 8$. In these

results $\Phi_1^B(\xi)$ is the leading-twist LCDAs of the B meson as defined by Eq. (14).

Weak annihilation contributions.—The basic building blocks for annihilation contributions originate from Fig. 3 and are given by (omitting the argument $M_1 M_2$ for brevity)

$$A_1^i = \pi\alpha_s \int_0^1 dudv\left\{\Phi_{M_2}(u)\Phi_{M_1}(v)\left[\frac{1}{v(1 - u\bar{v})} + \frac{1}{\bar{u}^2 v}\right]\right.$$
$$\left. + r_\chi^{M_1}r_\chi^{M_2}\Phi_p^{M_2}(u)\Phi_p^{M_1}(v)\frac{2}{\bar{u}v}\right\},$$

$$A_1^f = 0,$$

$$A_2^i = \pi\alpha_s \int_0^1 dudv\left\{\Phi_{M_2}(u)\Phi_{M_1}(v)\left[\frac{1}{\bar{u}(1 - u\bar{v})} + \frac{1}{\bar{u}v^2}\right]\right.$$
$$\left. + r_\chi^{M_1}r_\chi^{M_2}\Phi_p^{M_2}(u)\Phi_p^{M_1}(v)\frac{2}{\bar{u}v}\right\},$$

$$A_2^f = 0,$$

$$A_3^i = \pi\alpha_s \int_0^1 dudv\left\{r_\chi^{M_1}\Phi_{M_2}(u)\Phi_p^{M_1}(v)\frac{2\bar{v}}{\bar{u}v(1 - u\bar{v})}\right.$$
$$\left. - r_\chi^{M_2}\Phi_{M_1}(v)\Phi_p^{M_2}(u)\frac{2u}{\bar{u}v(1 - u\bar{v})}\right\},$$

$$A_3^f = \pi\alpha_s \int_0^1 dudv\left\{r_\chi^{M_1}\Phi_{M_2}(u)\Phi_p^{M_1}(v)\frac{2(1 + \bar{u})}{\bar{u}^2 v}\right.$$
$$\left. + r_\chi^{M_2}\Phi_{M_1}(v)\Phi_p^{M_2}(u)\frac{2(1 + v)}{\bar{u}v^2}\right\}, \tag{A11}$$

where the superscripts "i" and "f" refer to gluon emission from the initial and final-state quarks, respectively. The subscript "k" refers to one of the three possible Dirac structures $\Gamma_1 \otimes \Gamma_2$, i.e., $k = 1$ for $(V - A) \otimes (V - A)$, $k = 2$ for $(V - A) \otimes (V + A)$, and $k = 3$ for $(-2) \times (S - P) \otimes (S + P)$.

Considering the off-shellness of the gluon in Figs. 2 and 3, it is reasonable to evaluate the vertex and penguin corrections at the scale $\mu \sim m_b$, with the hard spectator scattering and the weak annihilation contributions at the scale $\mu_h = \sqrt{\Lambda_h \mu}$ with $\Lambda_h = 0.5$ GeV.

APPENDIX B: ANALYTIC EXPRESSIONS FOR THE Δ_i FUNCTIONS

In the NDR scheme, after performing the loop-momentum integration, we can present the analytic expressions for the Δ_i functions appearing in Eqs. (38) and (39) as

$$\Delta i_5 = -\Gamma\left(\frac{\epsilon}{2}\right)(4\pi\mu^2)^{\epsilon/2}\int_0^1 dx \int_0^{1-x} dy\, C^{-1-(\epsilon/2)}[2m_q^2\epsilon - 2m_q^2 x\epsilon - 2k^2 x^2\epsilon + 2k^2 x^3\epsilon + 2p^2 y\epsilon - 2p^2 y^2\epsilon + 2p^2 xy^2\epsilon$$
$$+ 4(k \cdot p)xy\epsilon - 4(k \cdot p)x^2 y\epsilon + 4C - 12Cx - 4Cx\epsilon], \tag{B1}$$

$$\Delta i_6 = \Gamma\!\left(\frac{\epsilon}{2}\right)(4\pi\mu^2)^{\epsilon/2} \int_0^1 dx \int_0^{1-x} dy\, C^{-1-(\epsilon/2)}[2m_q^2\epsilon + 2k^2x\epsilon - 2k^2x^2\epsilon - 2m_q^2y\epsilon + 2k^2x^2y\epsilon - 2p^2y^2\epsilon + 2p^2y^3\epsilon$$
$$+ 4(k\cdot p)xy\epsilon - 4(k\cdot p)xy^2\epsilon + 4C - 12Cy - 4Cy\epsilon], \tag{B2}$$

$$\Delta i_{23} = 4\Gamma\!\left(\frac{\epsilon}{2}\right)(4\pi\mu^2)^{\epsilon/2}(k\cdot p)\epsilon \int_0^1 dx \int_0^{1-x} dy\, C^{-1-(\epsilon/2)}xy, \tag{B3}$$

$$\Delta i_{24} = 4\Gamma\!\left(\frac{\epsilon}{2}\right)(4\pi\mu^2)^{\epsilon/2}(k\cdot p)\epsilon \int_0^1 dx \int_0^{1-x} dy\, C^{-1-(\epsilon/2)}y(1-y), \tag{B4}$$

$$\Delta i_{25} = -4\Gamma\!\left(\frac{\epsilon}{2}\right)(4\pi\mu^2)^{\epsilon/2}(k\cdot p)\epsilon \int_0^1 dx \int_0^{1-x} dy\, C^{-1-(\epsilon/2)}x(1-x), \tag{B5}$$

$$\Delta i_{26} = -\Delta i_{23}, \tag{B6}$$

$$\Delta i_2 = \Gamma\!\left(\frac{\epsilon}{2}\right)(4\pi\mu^2)^{\epsilon/2} \int_0^1 dx \int_0^{1-x} dy\, C^{-1-(\epsilon/2)}[2m_q^2\epsilon - 2m_q^2x\epsilon - 2k^2x^2\epsilon + 2k^2x^3\epsilon + 2p^2y\epsilon - 2p^2y^2\epsilon + 2p^2xy^2\epsilon$$
$$+ 4(k\cdot p)xy\epsilon - 4(k\cdot p)x^2y\epsilon + 4C - 4Cx - 4C\epsilon + 4Cx\epsilon], \tag{B7}$$

$$\Delta i_3 = -\Gamma\!\left(\frac{\epsilon}{2}\right)(4\pi\mu^2)^{\epsilon/2} \int_0^1 dx \int_0^{1-x} dy\, C^{-1-(\epsilon/2)}[2m_q^2\epsilon + 2k^2x\epsilon - 2k^2x^2\epsilon - 2m_q^2y\epsilon + 2k^2x^2y\epsilon - 2p^2y^2\epsilon + 2p^2y^3\epsilon$$
$$+ 4(k\cdot p)xy\epsilon - 4(k\cdot p)xy^2\epsilon + 4C - 4Cy - 4C\epsilon + 4Cy\epsilon], \tag{B8}$$

$$\Delta i_8 = -\Gamma\!\left(\frac{\epsilon}{2}\right)(4\pi\mu^2)^{\epsilon/2} \int_0^1 dx \int_0^{1-x} dy\, C^{-1-(\epsilon/2)}[2m_q^2\epsilon + 2m_q^2x\epsilon + 2k^2x^2\epsilon - 2k^2x^3\epsilon + 2p^2y\epsilon - 2p^2y^2\epsilon - 2p^2xy^2\epsilon$$
$$+ 4(k\cdot p)x^2y\epsilon + 4C + 4Cx - 4C\epsilon - 4Cx\epsilon], \tag{B9}$$

$$\Delta i_9 = -\Gamma\!\left(\frac{\epsilon}{2}\right)(4\pi\mu^2)^{\epsilon/2} \int_0^1 dx \int_0^{1-x} dy\, C^{-1-(\epsilon/2)}[2m_q^2\epsilon + 2k^2x\epsilon - 2k^2x^2\epsilon - 2m_q^2y\epsilon - 4k^2xy\epsilon + 2k^2x^2y\epsilon - 2p^2y^2\epsilon$$
$$+ 2p^2y^3\epsilon - 4(k\cdot p)y\epsilon + 4(k\cdot p)xy\epsilon + 4(k\cdot p)y^2\epsilon - 4(k\cdot p)xy^2\epsilon + 4C - 4Cy - 4C\epsilon + 4Cy\epsilon], \tag{B10}$$

$$\Delta i_{11} = \Gamma\!\left(\frac{\epsilon}{2}\right)(4\pi\mu^2)^{\epsilon/2} \int_0^1 dx \int_0^{1-x} dy\, C^{-1-(\epsilon/2)}[2m_q^2\epsilon - 2m_q^2x\epsilon - 2k^2x^2\epsilon + 2k^2x^3\epsilon + 2p^2y\epsilon - 4p^2xy\epsilon - 2p^2y^2\epsilon$$
$$+ 2p^2xy^2\epsilon - 4(k\cdot p)x\epsilon + 4(k\cdot p)x^2\epsilon + 4(k\cdot p)xy\epsilon - 4(k\cdot p)x^2y\epsilon + 4C - 4Cx - 4C\epsilon + 4Cx\epsilon], \tag{B11}$$

$$\Delta i_{12} = \Gamma\!\left(\frac{\epsilon}{2}\right)(4\pi\mu^2)^{\epsilon/2} \int_0^1 dx \int_0^{1-x} dy\, C^{-1-(\epsilon/2)}[2m_q^2\epsilon + 2k^2x\epsilon - 2k^2x^2\epsilon + 2m_q^2y\epsilon - 2k^2x^2y\epsilon + 2p^2y^2\epsilon - 2p^2y^3\epsilon$$
$$+ 4(k\cdot p)xy^2\epsilon + 4C + 4Cy - 4C\epsilon - 4Cy\epsilon], \tag{B12}$$

$$\Delta i_{15} = 8\Gamma\!\left(\frac{\epsilon}{2}\right)(4\pi\mu^2)^{\epsilon/2}(k\cdot p)\epsilon \int_0^1 dx \int_0^{1-x} dy\, C^{-1-(\epsilon/2)}(1-x)x^2, \tag{B13}$$

$$\Delta i_{16} = 4\Gamma\!\left(\frac{\epsilon}{2}\right)(4\pi\mu^2)^{\epsilon/2}(k\cdot p)\epsilon \int_0^1 dx \int_0^{1-x} dy\, C^{-1-(\epsilon/2)}x(1-x)(1-2y), \tag{B14}$$

$$\Delta i_{17} = -4\Gamma\!\left(\frac{\epsilon}{2}\right)(4\pi\mu^2)^{\epsilon/2}(k\cdot p)\epsilon \int_0^1 dx \int_0^{1-x} dy\, C^{-1-(\epsilon/2)}xy(1-2x), \tag{B15}$$

$$\Delta i_{18} = -4\Gamma\!\left(\frac{\epsilon}{2}\right)(4\pi\mu^2)^{\epsilon/2}(k\cdot p)\epsilon \int_0^1 dx \int_0^{1-x} dy\, C^{-1-(\epsilon/2)}y(1-x-y+2xy), \tag{B16}$$

$$\Delta i_{19} = 4\Gamma\left(\frac{\epsilon}{2}\right)(4\pi\mu^2)^{\epsilon/2}(k \cdot p)\epsilon \int_0^1 dx \int_0^{1-x} dy C^{-1-(\epsilon/2)} x(1 - x - y + 2xy), \tag{B17}$$

$$\Delta i_{20} = -4\Gamma\left(\frac{\epsilon}{2}\right)(4\pi\mu^2)^{\epsilon/2}(k \cdot p)\epsilon \int_0^1 dx \int_0^{1-x} dy C^{-1-(\epsilon/2)}(1 - 2x)y(1 - y), \tag{B18}$$

$$\Delta i_{21} = 4\Gamma\left(\frac{\epsilon}{2}\right)(4\pi\mu^2)^{\epsilon/2}(k \cdot p)\epsilon \int_0^1 dx \int_0^{1-x} dy C^{-1-(\epsilon/2)} xy(1 - 2y), \tag{B19}$$

$$\Delta i_{22} = -8\Gamma\left(\frac{\epsilon}{2}\right)(4\pi\mu^2)^{\epsilon/2}(k \cdot p)\epsilon \int_0^1 dx \int_0^{1-x} dy C^{-1-(\epsilon/2)}(1 - y)y^2, \tag{B20}$$

where the parameter C is defined by

$$C = m_q^2 - x(1 - x)k^2 - y(1 - y)p^2 - 2xy(k \cdot p) - i\delta, \tag{B21}$$

with m_q being the quark mass in the fermion loops.

For a B meson decaying into two light energetic hadronic final states, the characteristic scale for the quark momentum of the final-state meson constituents is of order m_b, whereas the momentum of the spectator quark from the B meson is of order Λ_{QCD}. Assuming that the off-shell gluon with index (ν, b, p) is connected with the spectator quark in the B meson, at leading power in Λ_{QCD}/m_b, the Δi functions given above can then be simplified greatly. After subtracting the regulator ϵ using the $\overline{\text{MS}}$ scheme and performing the Feynman parameter integrals, we get (here we give only the relevant Δi functions needed in this paper; details for the others can be found in Ref. [47])

$$\Delta i_5 = 2 + \frac{2r_1}{r_3}[G_0(r_1) - G_0(r_1 + r_3)] - \frac{4}{r_3}[G_{-1}(r_1) - G_{-1}(r_1 + r_3)], \tag{B22}$$

$$\Delta i_6 = -2 - \frac{4}{r_3} + \frac{2r_1(1 + r_3)}{r_3^2}G_0(r_1) - \frac{2(r_1 + r_3 + r_1 r_3)}{r_3^2}G_0(r_1 + r_3) + \frac{4}{r_3}[G_{-1}(r_1) - G_{-1}(r_1 + r_3)]$$
$$- \frac{(4 - r_1)r_1}{r_3^2}T_0(r_1) + \frac{(4 - r_1 - r_3)(r_1 + r_3)}{r_3^2}T_0(r_1 + r_3), \tag{B23}$$

$$\Delta i_{23} = -2 - \frac{2r_1}{r_3}[G_0(r_1) - G_0(r_1 + r_3)] + \frac{4}{r_3}[G_{-1}(r_1) - G_{-1}(r_1 + r_3)], \tag{B24}$$

$$\Delta i_{26} = -\Delta i_{23}, \tag{B25}$$

$$\Delta i_2 = -\frac{22}{9} + \frac{8}{3}\ln\frac{\mu}{m_c} - \frac{2(8 + r_1)}{3r_3}G_0(r_1) + \frac{2(8 + r_1 - 2r_3)}{3r_3}G_0(r_1 + r_3) + \frac{4}{r_3}[G_{-1}(r_1) - G_{-1}(r_1 + r_3)], \tag{B26}$$

$$\Delta i_3 = \frac{22}{9} + \frac{12}{r_3} + \frac{4r_1}{3r_3} - \frac{8}{3}\ln\frac{\mu}{m_c} - \frac{2(7r_1 - r_3 - 3r_1 r_3 + 2r_1^2 - 2r_3^2)}{3r_3^2}G_0(r_1 + r_3) + \frac{2r_1(7 + 2r_1 - 3r_3)}{3r_3^2}G_0(r_1)$$
$$- \frac{4(2r_1 + r_3)}{r_3^2}[G_{-1}(r_1) - G_{-1}(r_1 + r_3)] + \frac{3(4 - r_1)r_1}{r_3^2}T_0(r_1) - \frac{3(4 - r_1 - r_3)(r_1 + r_3)}{r_3^2}T_0(r_1 + r_3), \tag{B27}$$

$$\Delta i_8 = \frac{32}{9} - \frac{16}{3}\ln\frac{\mu}{m_c} - \frac{8(2 + r_1)}{3r_3}G_0(r_1) + \frac{8(2 + r_1 + r_3)}{3r_3}G_0(r_1 + r_3), \tag{B28}$$

$$\Delta i_{12} = -\frac{32}{9} + \frac{12}{r_3} + \frac{4r_1}{3r_3} + \frac{16}{3}\ln\frac{\mu}{m_c} + \frac{2r_1(7 + 2r_1 + 6r_3)}{3r_3^2}G_0(r_1) - \frac{2(2r_1^2 - r_3(1 - 4r_3) + r_1(7 + 6r_3))}{3r_3^2}G_0(r_1 + r_3)$$
$$- \frac{8r_1}{r_3^2}[G_{-1}(r_1) - G_{-1}(r_1 + r_3)] + \frac{3(4 - r_1)r_1}{r_3^2}T_0(r_1) - \frac{3(4 - r_1 - r_3)(r_1 + r_3)}{r_3^2}T_0(r_1 + r_3), \tag{B29}$$

$$\Delta i_{17} = \frac{2}{3} + \frac{2(8 + r_1)}{3r_3}G_0(r_1) - \frac{2}{3}\left(\frac{8 + r_1}{r_3} + \frac{4}{r_1 + r_3}\right)G_0(r_1 + r_3) - \frac{4}{r_3}[G_{-1}(r_1) - G_{-1}(r_1 + r_3)], \quad \text{(B30)}$$

$$\Delta i_{21} = -\frac{2}{3} - \frac{16}{r_3} - \frac{8r_1}{3r_3} + \frac{2r_1(4r_1^2 + 3r_3(8 + r_3) + r_1(20 + 7r_3))}{3r_3^2(r_1 + r_3)}G_0(r_1 + r_3) - \frac{2r_1(20 + 4r_1 + 3r_3)}{3r_3^2}G_0(r_1)$$

$$+ \frac{4(4r_1 + r_3)}{r_3^2}[G_{-1}(r_1) - G_{-1}(r_1 + r_3)] - \frac{4(4 - r_1)r_1}{r_3^2}T_0(r_1) + \frac{4(4 - r_1 - r_3)(r_1 + r_3)}{r_3^2}T_0(r_1 + r_3), \quad \text{(B31)}$$

where we have introduced the notations $r_1 = k^2/m_q^2$, $r_2 = p^2/m_q^2$, and $r_3 = 2(k \cdot p)/m_q^2$, with $m_q = m_c$ or m_b. For light u, d, s quark loops, these Δi functions can be evaluated straightforwardly.

The functions $G_i(t)(i = -1, 0)$ are defined by

$$G_i(t) = \int_0^1 dx x^i \ln[1 - x(1 - x)t - i\delta]. \quad \text{(B32)}$$

The explicit form for $G_{-1,0}(t)$ can be found in Ref. [45].

In addition, we have also introduced the function $T_i(t)$, which is defined by

$$T_i(t) = \int_0^1 dx \frac{x^i}{1 - x(1 - x)t - i\delta}. \quad \text{(B33)}$$

The explicit form for $T_0(t)$ is given by [47]

$$T_0(t) = \begin{cases} \frac{4\arctan\sqrt{\frac{t}{4-t}}}{\sqrt{t(4-t)}}; & 0 \le t \le 4 \\ \frac{2i\pi + 2\ln(\sqrt{t} - \sqrt{t-4}) - 2\ln(\sqrt{t} + \sqrt{t-4})}{\sqrt{t(t-4)}}; & t > 4. \end{cases} \quad \text{(B34)}$$

[1] M. Bauer, B. Stech, and M. Wirbel, Z. Phys. C **29**, 637 (1985); Z. Phys. C **34**, 103 (1987).

[2] T. W. Yeh and H-n. Li, Phys. Rev. D **56**, 1615 (1997); Y. Y. Keum, H-n. Li, and A. I. Sanda, Phys. Lett. B **504**, 6 (2001); Phys. Rev. D **63**, 054008 (2001); Y. Y. Keum and H-n. Li, Phys. Rev. D **63**, 074006 (2001).

[3] M. Beneke, G. Buchalla, M. Neubert, and C. T. Sachrajda, Phys. Rev. Lett. **83**, 1914 (1999); Nucl. Phys. **B591**, 313 (2000).

[4] M. Neubert, AIP Conf. Proc. **602**, 168 (2001); AIP Conf. Proc. **618**, 217 (2002).

[5] C. W. Bauer, D. Pirjol, and I. W. Stewart, Phys. Rev. Lett. **87**, 201806 (2001); Phys. Rev. D **65**, 054022 (2002); **67**, 071502 (2003); J. Chay and C. Kim, Phys. Rev. D **65**, 114016 (2002); M. Beneke, A. P. Chapovsky, M. Diehl, and T. Feldmann, Nucl. Phys. **B643**, 431 (2002).

[6] D. Cronin-Hennessy et al. (CLEO Collaboration), Phys. Rev. Lett. **85**, 515 (2000).

[7] D. M. Asner et al. (CLEO Collaboration), Phys. Rev. D **65**, 031103 (2002).

[8] A. Bornheim et al. (CLEO Collaboration), Phys. Rev. D **68**, 052002 (2003).

[9] BABAR Collaboration, http://www-public.slac.stanford.edu/babar/BaBarPublications.

[10] Belle Collaboration, http://belle.kek.jp.

[11] S. Chen et al. (CLEO Collaboration), Phys. Rev. Lett. **85**, 525 (2000).

[12] K. Abe et al. (Belle Collaboration), Phys. Rev. Lett. **93**, 021601 (2004).

[13] B. Aubert et al. (BABAR Collaboration), Phys. Rev. Lett. **93**, 131801 (2004).

[14] M. Giorgi, in Proceedings of the 32nd International Conference on High Energy Physics, Beijing, China, 2004, edited by H. S. Chen, D. S. Du, W. G. Li, and C. D. Lu (World Scientific, Singapore, 2004).

[15] Y. Chao and P. Chang (Belle Collaboration), Phys. Rev. D **71**, 031502 (2005).

[16] Y. Chao et al. (Belle Collaboration), Phys. Rev. Lett. **93**, 191802 (2004).

[17] K. Abe et al. (Belle Collaboration), hep-ex/0409049.

[18] B. Aubert et al. (BABAR Collaboration), Phys. Rev. Lett. **94**, 181802 (2005).

[19] Y. Chao et al. (Belle Collaboration), Phys. Rev. Lett. **94**, 181803 (2005).

[20] Y. Sakai, in Ref. [14].

[21] M. Beneke, G. Buchalla, M. Neubert, and C. T. Sachrajda, Nucl. Phys. **B606**, 245 (2001).

[22] T. Muta, A. Sugamoto, M. Z. Yang, and Y. D. Yang, Phys. Rev. D **62**, 094020 (2000).

[23] D.-s. Du, D.-s. Yang, and G.-h. Zhu, Phys. Lett. B **488**, 46 (2000).

[24] D.-s. Du, H.-j. Gong, J.-f. Sun, D.-s. Yang, and G.-h. Zhu, Phys. Rev. D **65**, 074001 (2002).

[25] M. Beneke, G. Buchalla, M. Neubert, and C. T. Sachrajda, Nucl. Phys. **B675**, 333 (2003).

[26] R. Fleischer and T. Mannel, Phys. Rev. D **57**, 2752 (1998).

[27] A. J. Buras and R. Fleischer, Eur. Phys. J. C **11**, 93 (1999).

[28] Heavy Flavor Averaging Group, http://www.slac.stanford.edu/xorg/hfag.

[29] A. J. Buras and R. Fleischer, Eur. Phys. J. C **16**, 97 (2000).

[30] A. J. Buras, R. Fleischer, S. Recksiegel, and F. Schwab, Phys. Rev. Lett. **92**, 101804 (2004); Nucl. Phys. **B697**, 133

(2004); Acta Phys. Pol. B **36**, 2015 (2005); hep-ph/0411373.

[31] S. Mishima and T. Yoshikawa, Phys. Rev. D **70**, 094024 (2004).

[32] Y. L. Wu and Y. F. Zhou, Phys. Rev. D **71**, 021701 (2005).

[33] Y. Y. Charng and H. n. Li, Phys. Rev. D **71**, 014036 (2005).

[34] X. G. He and B. H. J. McKellar, hep-ph/0410098.

[35] S. Baek, P. Hamel, D. London, A. Datta, and D. A. Suprun, Phys. Rev. D **71**, 057502 (2005).

[36] T. Carruthers and B. H. J. McKellar, hep-ph/0412202.

[37] S. Nandi and A. Kundu, hep-ph/0407061.

[38] T. Morozumi, Z. H. Xiong, and T. Yoshikawa, hep-ph/0408297.

[39] C. N. Burrell and A. R. Williamson, hep-ph/0504024.

[40] C. S. Kim, S. Oh, and C. Yu, hep-ph/0505060 [Phys. Rev. D (to be published)].

[41] T. W. Yeh, hep-ph/0506181.

[42] W. S. Hou, Nucl. Phys. **B308**, 561 (1988).

[43] J.-M. Gérard and W. S. Hou, Phys. Rev. Lett. **62**, 855 (1989); Phys. Rev. D **43**, 2909 (1991); Phys. Lett. B **253**, 478 (1991).

[44] H. Simma and D. Wyler, Nucl. Phys. **B344**, 283 (1990); J. Liu and Y. P. Yao, Phys. Rev. D **41**, 2147 (1990).

[45] C. Greub and P. Liniger, Phys. Rev. D **63**, 054025 (2001).

[46] S. W. Bosch and G. Buchalla, Nucl. Phys. **B621**, 459 (2002); M. Beneke, T. Feldmann, and D. Seidel, Nucl. Phys. **B612**, 25 (2001); A. Ali and A. Y. Parkhomenko, Eur. Phys. J. C **23**, 89 (2002).

[47] G. Eilam and Y. D Yang, Phys. Rev. D **66**, 074010 (2002).

[48] S. Mishima and A. I. Sanda, Prog. Theor. Phys. **110**, 549 (2003).

[49] G. Buchalla, A. J. Buras, and M. E. Lautenbacher, Rev. Mod. Phys. **68**, 1125 (1996).

[50] A. J. Buras, hep-ph/9806471; Lect. Notes Phys. **558**, 65 (2000).

[51] C. D. Lü, K. Ukai, and M. Z. Yang, Phys. Rev. D **63**, 074009 (2001).

[52] A. Kagan, Phys. Lett. B **601**, 151 (2004).

[53] M. Beneke and T. Feldmann, Nucl. Phys. **B592**, 3 (2001); M. Beneke, Nucl. Phys. B, Proc. Suppl. **111**, 62 (2002).

[54] A. G. Grozin and M. Neubert, Phys. Rev. D **55**, 272 (1997).

[55] B. V. Geshkenbein and M. V. Terentev, Yad. Fiz. **40**, 758 (1984) [Sov. J. Nucl. Phys. **40**, 487 (1984)].

[56] P. Ball and V. M. Braun, Phys. Rev. D **58**, 094016 (1998); P. Ball, J. High Energy Phys. 09 (1998) 005.

[57] M. Bander, D. Silverman, and A. Soni, Phys. Rev. Lett. **43**, 242 (1979).

[58] A. J. Buras, P. Gambino, and U. A. Haisch, Nucl. Phys. **B570**, 117 (2000).

[59] L. Wolfenstein, Phys. Rev. Lett. **51**, 1945 (1983).

[60] S. Eidelman *et al.*, Phys. Lett. B **592**, 1 (2004).

[61] V. M. Braun and I. E. Filyanov, Z. Phys. C **48**, 239 (1990).

[62] T. Feldmann and T. Hurth, J. High Energy Phys. 11 (2004) 037.

[63] V. M. Braun, D. Y. Ivanov, and G. P. Korckemsky, Phys. Rev. D **69**, 034014 (2004).

[64] A. Khodjamirian, T. Mannel, and N. Offen, Phys. Lett. B **620**, 52 (2005).

[65] P. Ball and R. Zwicky, Phys. Rev. D **71**, 014015 (2005).

[66] K. Abe (Belle Collaboration), in *Proceedings of the Lake Louise Winter Institute 2004, Canada*, http://www.phys.ualberta.ca/~llwi.

[67] H. n. Li, S. Mishima, and A. I. Sanda, hep-ph/0508041.